On *Dracograllus miguelitus* sp. nov. (Nematoda: Draconematidae) from an inactive structure: insights into its taxonomy, biodiversity and ecology at hydrothermal vents

William Johnson da Silva[1], Daniela Zeppilli[1], Valentin Foulon[2], Pierre-Antoine Dessandier[1], Marjolaine Matabos[1] and Jozee Sarrazin[1]

[1] Ifremer, BEEP, Univ Brest, Plouzané, France
[2] ENIB—École Nationale d'Ingénieurs de Brest, Plouzané, France

ABSTRACT

Background: Hydrothermal vent fields are habitats to a diverse array of benthic organisms, including several nematode species, which represent a significant portion of the biodiversity in these environments. Despite their ecological importance, most research on hydrothermal vents has focused on macro-invertebrates. As a result, vent nematode biodiversity remains largely unexplored, especially in peripheral and inactive structures, underscoring the need for further investigation. A sampling program conducted in 2017 and 2018 along a gradient of venting activity led to the collection of a number of Draconematidae species in various habitats. In this article, we introduce *Dracograllus miguelitus* sp. nov., the first species of the genus described at a hydrothermal vent field, sampled from a visually inactive sulphide structure.

Methods: The samples were collected at the Lucky Strike vent field, on the Mid-Atlantic Ridge, using the suction sampler of the Remotely Operated Vehicle Victor6000. Specimens were retrieved from an edifice covered by a black layer of manganese oxy-hydroxides, with no local visible hydrothermal activity, at a depth of 1.639 m. Samples were sieved on a 32 μm mesh onboard, sorted and, for nematodes, identified to species level back in the lab. Fluorescent images were obtained using the ApoTome Fluorescence Microscope Module, and 3D observations were possible through the depth change method.

Results: We established *D. miguelitus* sp. nov. as a new species based on the combination of the following characters: four cephalic adhesive tubes (CATs), an elongated loop-shaped amphid with varying branch sizes between males and females, and a circular amphid in juveniles. Additionally, females display a minute setae emerging from the vulvar aperture. In males, the posterior adhesive tubes (PATs) are arranged in four longitudinal rows: two sublateral rows, each containing 10–12 PATs, and two subventral rows, consisting of 10 PATs in each. In females, sublateral and subventral rows with 13 PATs each. So far, *D. miguelitus* sp. nov. is the first species of the genus to be described from a hydrothermal environment and the deepest one. Beyond the formal description of this new species, we provide ecological and taxonomic backgrounds on Draconematidae at hydrothermal vents, with insights into the genus distribution, biogeography, and nomenclatural issues.

Conclusion: This discovery contributes to the knowledge of Draconematidae biodiversity, and highlights the importance to investigate nematode communities at species-level, data that is often missing at vent studies. Additionally, it underscores the significance of preserving inactive hydrothermal habitats, which are threatened by deep-sea mining activities.

INTRODUCTION

A significant portion of the benthic diversity associated with hydrothermal vents is represented by nematodes, which play crucial roles at the ecosystem level such as bioturbation and organic matter degradation (*Vanreusel, Van den Bossche & Thiermann, 1997*; *Vanreusel et al., 2010a*, *2010b*). These environments are characterized by a hard substratum with high contents of metal compounds such as copper, zinc and iron, resulting from the precipitation of polymetallic sulphides contained in the vent fluids (*Hoagland et al., 2010*). Unlike other deep-sea ecosystems, hydrothermal vents exhibit a unique combination of low diversity and high biomass, largely driven by chemosynthetic energy sources (*Tunnicliffe, 1991*). Nematodes thrive in these conditions, highlighting their remarkable ability to adapt to habitat heterogeneity and extreme environments (*Vanreusel et al., 2010b*).

Surviving the peculiar environmental conditions of the deep sea, such as high pressure, low temperatures, and food scarcity, poses a significant challenge for faunal communities. Hydrothermal vents introduce further selective pressures linked to the type, origin, and intensity of hydrothermal activity and resulting environmental conditions (*Koschinsky et al., 2008*). Consequently, nematode communities at vents differ from those in the surrounding deep-sea. They harbor species that possess adaptations and strategies that are essential to survive in these harsh environments (*Vanreusel et al., 2010a*). Species diversity vary significantly across sites with different levels of hydrothermal activity (*Gollner, Miljutina & Bright, 2013*) and differences in species composition underscore their ability to occupy various niches, making them important contributors to the functioning of hydrothermal ecosystems (*Vanreusel et al., 2010b*).

Some examples of these adaptations can be observed in the Draconematidae family (*Filipjev, 1918*). These nematodes are easily recognizable by their S-shaped body morphology, which is common to most species. This unique shape has earned them colloquial names of "walking nematodes" or "dragon nematodes." In addition to their distinct morphology, many Draconematidae exhibit specialized structures that are closely tied to their locomotion and habitat use. Their cephalic (CATs) and posterior (PATs) adhesive tubes are linked to glands that secrete adhesive substances. These secretions allow them to "stick" parts of their bodies to the substratum, enabling alternative movements with intervals of "attachment and release" of both anterior and posterior body regions (*Stauffer, 1924*; *Cobb, 1929*; *Clasing, 1980*; *Tchesunov, 2014*). The Draconematidae family

comprises 16 genera and 89 valid species (*Nemys, 2024*), most of which are commonly found in coastal regions, typically associated with biological structures such as worm tubes, algae and coral reefs (*Decraemer, Gourbault & Backeljau, 1997*). The unexpected discovery of Draconematidae species in high abundances at hydrothermal vents was first reported in the Guaymas Basin on the East Pacific Rise (2,000 m water depth) by *Dinet, Grassle & Tunnicliffe (1988)*. Since then, additional records of the family in deep-sea habitats, including hydrothermal vents, have been reported. Several genera typical of deep-sea environments were collected, such as *Cephalochaetosoma* (syn. *Bathychaetosoma*) and *Dinetia* from the subfamily Draconematinae, as well as *Prochaetosoma* from the subfamily Prochaetosomatinae (*Kito, 1983*; *Decraemer, Gourbault & Backeljau, 1997*; *Rho, Kim & Min, 2007*; *Rho & Min, 2011*, and references therein). On the East Pacific Rise (EPR), *Dinetia* sp. were associated with *Bathymodiolus* mussel beds (*Flint et al., 2006*). Similarly, at the Lucky Strike vent field, along the northern Mid-Atlantic Ridge (MAR), both *Dinetia* and *Cephalochaetosoma* were associated with *Bathymodiolus* mussels (*Husson et al., 2017*). More recently, an experimental colonization study showed that *Cephalochaetosoma* represented between 76% and 90% of the nematode community on inorganic substrata deployed in intense vent emission areas (*Zeppilli et al., 2015*).

The genus *Dracograllus Allen & Noffsinger, 1978* represents the largest genus within the family, with 25 valid species (*Min et al., 2016*; *Nemys, 2024*), most of them reported in shallow waters, and, as for several Draconematidae species, associated with biogenic structures (*Verschelde & Vincx, 1993*). Even without apomorphic characters, the genus can be distinguished from other genera by several features, including a non-enlarged cuticle in the head region, the absence of bilateral cephalic acanthiform setae on the head capsule (except for *D. stekhoveni*), the absence of precloacal copulatory thorns, and the presence of paravulvar setae in some species (*Allen & Noffsinger, 1978*; *Decraemer, 1988*; *Decraemer, Gourbault & Backeljau, 1997*). Up to now, no species of *Dracograllus* had been formally described from deep-sea or hydrothermal habitats, as their distribution is generally limited to depths shallower than 100 m. However, several recent studies have reported *Dracograllus* specimens at greater depths (*Vanhove, Arntz & Vincx, 1999*; *Gad, 2009*; *Zeppilli et al., 2014*; *Spedicato et al., 2020*), although none have been formally described so far.

Most part of the vent ecological studies have focused on the microbial and macrofaunal compartments on active hydrothermal structures, neglecting the smaller meiofauna and also, the fauna from regions adjacent to the vents and inactive structures. However, although they received less attention, there is an increased interest in studying inactive vents, because they are the main target for mineral extraction (*Menini et al., 2023*). Recent studies have shown differences in faunal diversity between hydrothermally active and inactive habitats with a much higher diversity in the latter (*Cowart et al., 2020*). Few studies in the vent periphery have shown that nematode diversity extends outside the active zones (*Vanreusel et al., 2010b*). In this context, it becomes critical to better understand their diversity patterns in vent ecosystems including in their sphere of influence (*Levin et al., 2016*). Such knowledge is essential for developing environmental management plans to mitigate the impacts of deep-sea mining.

To assess meiofaunal benthic biodiversity associated with different vent environmental conditions, a sampling was carried out at 1,700 m depth at the Lucky Strike vent field in three contrasting habitats: an active vent site, a 'visually' inactive structure, and an area peripheral to venting activity (*Cowart et al., 2020*). In this study, we describe for the first time a new species of *Dracograllus* sampled from a deep-sea inactive sulfide structure, and supply updates on the taxonomy, ecology, and distribution of the genus. Additionally, we provide a dichotomous key to aid in the identification of *Dracograllus* species. Finally, we examine the implications of our results for the conservation of hydrothermal ecosystems, focusing on species composition, interactions and ecosystem functions in the context of the challenges posed by the mining industry.

MATERIALS AND METHODS

Study area and sampling collection

The Lucky Strike (LS) vent field is located in the northern part of the Mid-Atlantic Ridge (MAR), south of the Azores (Fig.1A), with a mean depth of 1,700 m (*De Busserolles et al., 2009*). LS consists of three volcanic cones that harbor over 25 active hydrothermal edifices surrounding a central lava lake (*Humphris et al., 2002*; *Ondreas et al., 2009*). Each active site-or edifice-is made of several smokers as well as patches of diffuse venting areas that extend in the periphery. To characterize the meiofaunal communities at the vent field scale, three habitat types were sampled: an active area, the periphery away from hydrothermal activity and a visually inactive edifice (Fig.1B).

The active habitat was located on the Montségur edifice (37°17.28′N, 32°16.53′W), in the southern region of LS, and consisted of cracks on a flat hydrothermal slab at the base of the edifice. The peripheral habitat was approximately 30 m from Montségur (37°17.28′N, 32°16.52′W), and covered by a few centimeters of sediments. Finally, the visually inactive structure, peripheral to the active Sintra edifice, lied about 400 m north of Montségur (37°17.48′N, 32°16.50′W), and consisted in an indurated sulfide structure covered at its base by a thin black layer of manganese oxy-hydroxides (Figs. 1C, 1D). Sampling was conducted during the 2018 Momarsat cruise (*Cannat, 2018*) using the suction sampler of the Remotely Operated Vehicle Victor6000. Neither the peripheral nor the inactive habitats exhibited visible hydrothermal activity or typical vent fauna. Once onboard, samples were sieved on 300 and 32 μm mesh sizes, and the fraction between 32–300 μm was preserved in 4% borax buffered formalin.

Sample preparation and image acquisition

Nematodes were extracted from the sediment by the use of colloidal silica (Ludox), with specific gravity of 1.39 (*Pfannkuche & Thiel, 1988*). Specimens were fixed in formalin, and after the (*De Grisse, 1969*) protocol, they were transferred to glycerol and mounted onto permanent slides (*Somerfield & Warwick, 1996*). Drawings and measurements were made using a light microscope Leica DM 2500 LED with the aid of a drawing tube and a Leica DMC 4500 camera.

For the fluorescent observations, a Zeiss Axio Imager.Z2 microscope equipped with an Colibri.7 light, an ORCAFlash4.OLT (Hamamatsu, Hamamatsu-city, Japan) camera and a
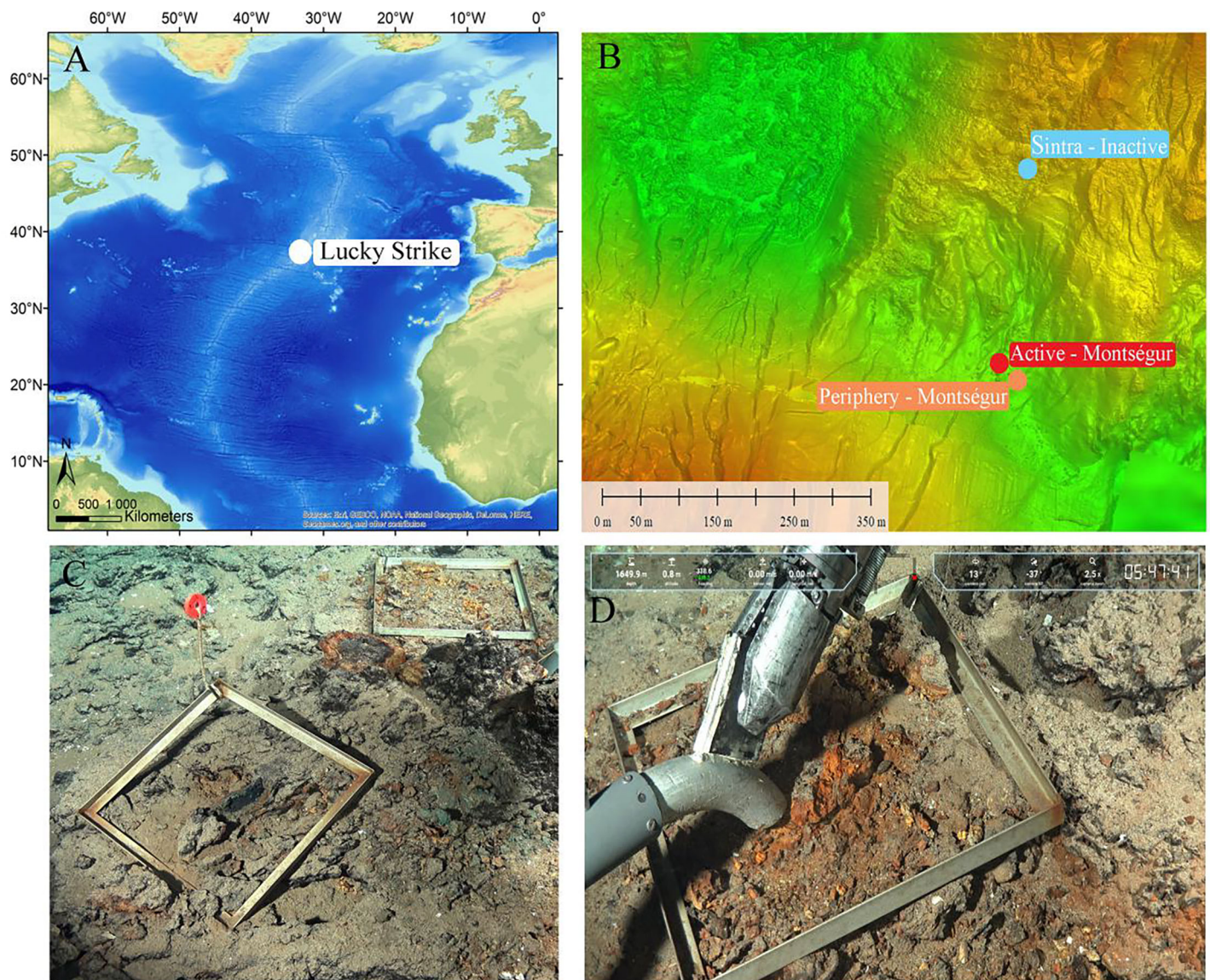
Figure 1 Study site and sampling approach. (A) Lucky Strike (LS) vent field along the Mid-Atlantic Ridge (MAR). (B) The three contrasting sampling sites. (C, D) Quadrats, faunal sampling and substratum view at the inactive habitat at LS. Source: Victor6000, Momarsat 2018, Ifremer. LS map modified from *Husson et al. (2017)*. Full-size 🖼 DOI: 10.7717/peerj.19585/fig-1

Apotome.2 slider module (for optical sections) was used. Autofluorescence and Phloxine B stain (Exitation 561 nm, Emission 571 nm) were used to observe internal and external structures in 3D. Thus, four fluorescent channels were used: Blue-filter Zeiss 49 DAPI Ex. G365 nm, Em. 445/50 nm, Green-filter Zeiss 38 HE GFP Ex 470/40 nm, Em LP 515 nm, Orange-filter Zeiss 43HE dsREd Ex. 550/25 nm Em. 605/70 nm, Red-filter Zeiss 50Cy5 Ex. 640/30 Em. 690/50 nm. Combinations of one to five channels (with brightfield) were used for optical section, increased depth of field and 3D depending on the observations. Images were processed using Zeiss Zen Pro and Arivis 4D Pro software.

In one of the earliest reviews of Draconematidae, *Allen & Noffsinger (1978)* provided key recommendations regarding specimen measurements, morphological analysis, and species delimitation. Building on their guidance, this study incorporates the following recommendations and observations: (1) measurements on the CATs should be taken on the right side of the nematode, (2), the length of the swollen esophageal and cephalic regions should be measured from the anterior tip of the lip region to just posterior to the swollen esophageal region (in most Draconematidae, the body is constricted in this region), (3) the body diameter width should be measured at the widest part of the swollen esophageal region while (4) the rostral width should be measured at the base of the rostrum, just anterior to the first body annule. For comprehensive details about measurements and possible variations along developmental stages, see *Allen & Noffsinger (1978)* and *Clasing (1980)*.

Nomenclatural acts

The electronic version of this article in Portable Document Format (PDF) will represent a published work according to the International Commission on Zoological Nomenclature (ICZN), and hence the new names contained in the electronic version are effectively published under that Code from the electronic edition alone. This published work and the nomenclatural acts it contains have been registered in ZooBank, the online registration system for the ICZN. The ZooBank LSIDs (Life Science Identifiers) can be resolved and the associated information viewed through any standard web browser by appending the LSID to the prefix http://zoobank.org/. The LSID for this publication is: (AA6564D7-6BA7-405E-94D3-B659E62B8BDB). The online version of this work is archived and available from the following digital repositories: PeerJ, PubMed Central SCIE and CLOCKSS.

RESULTS AND DISCUSSION

This is the first study to describe a new *Dracograllus* species from an inactive vent structure. It also corresponds to the greatest depth recorded among all known congener valid species. This finding provides insights into the diversity of potential habitats for Draconematidae, with genera and species distributed across a wide range of environments from shallow to deep regions.

SYSTEMATICS

Class CHROMADOREA *Inglis, 1983*
Subclass CHROMADORIA *Pearse, 1942*
Order Desmodorida *De Coninck, 1965*
Suborder Desmodorina *De Coninck, 1965*
Superfamily Desmodoroidea *Filipjev, 1922*
Family Draconematidae *Filipjev, 1918*

Diagnosis. (Emended from *Leduc & Zhao (2016)*): Body short, S-shaped, usually with more or less enlarged pharyngeal and mid-body region. Cuticle annulated except for the head capsule (helmet) and tail terminus. Annules sometimes with spines, minute vacuoles, or a longitudinal lateral field in mid-body region or tail region. Cephalic sensilla in three

circles (6 + 6 + 4): six inner labial papillae, six outer labial setae, and four cephalic setae. Rostrum present (except in *Dinetia*). Amphideal fovea spiral to loop-shaped, rarely reduced or an internal longitudinal bar. CATs present, located dorsally on the cephalic capsule. Somatic setae arranged in eight longitudinal rows. Buccal cavity small to well developed, usually with a dorsal tooth, with or without subventral teeth. Pharynx cylindrical, dumbbell shaped, or with posterior bulb. Secretory–excretory system absent. At least the anterior-most PATs are arranged in four longitudinal rows, two subventrally and two ventrosublaterally, located on the posterior third of the body. PATs with or without differentiated tips, usually straight, rarely long and flexible. Copulatory apparatus with two spicules and trough-shaped gubernaculum. Three caudal glands extending beyond anus/cloaca.

Subfamily Draconematinae Filipjev, 1918

Diagnosis. (Emended from *Decraemer, Gourbault & Backeljau (1997)*): Pharynx dumbbell-shaped. Swollen anterior body region is usually conspicuous and short. CATs with clearly open tips, mainly blister-shaped, and enlarged bases of insertion, located on the rostrum. Cephalic acanthiform setae may be present on the helmet. Buccal cavity narrow, unarmed. PATs shorts and straights (except for *Draconema trispinosum*, characterized by some longer tubes), with bell-shaped tips. All PATs are anterior to cloaca (except in *Dracograllus eira* and *Dracograllus minutus*). Copulatory thorns are rare. Paravulvar setae present or not. Tail cylindro-conoid with numerous nodules. Non-annulated tail region, with different length between species.

Type genus. *Draconema* Cobb, 1913.
Genus *Dracograllus* Allen & Noffsinger, 1978

Diagnosis. (Emended from *Leduc & Zhao (2016)*): Draconematidae, Draconematinae. Swollen anterior body region 18–26% of total body length. Usually eight CATs on the helmet, rarely 10 to 15. Non-enlarged cuticle on the rostrum. Amphids lateral, usually loop-shaped, with branches usually of unequal length, rarely spiral. Precloacal copulatory thorns are usually absent. PATs all anterior to cloacal opening (except in *Dracograllus eira Inglis, 1968* and *Dracograllus minutus Decraemer, 1988*), and usually extending posterior to anus in females (four exceptions). Paravulvar setae may be present.

Type species. *Dracograllus cobbi* Allen & Noffsinger, 1978.

Remarks on *Dracograllus* taxonomy. The genus *Dracograllus* is placed within the subfamily Draconematinae, along with *Draconema, Paradraconema*, and also the genus *Tenuidraconema*. On the other hand, the subfamily Prochaetosomatinae includes the deep-sea typical genera: *Bathychaetosoma, Cephalochaetosoma*, and *Dinetia*, as well as *Prochaetosoma*. This classification is based on characteristics such as the cylindrical shape of the pharyngeal sphincter with a terminal bulb, suggesting that the typical dumbbell-shaped pharynx was possibly secondarily lost in *Tenuidraconema* (*Decraemer, Gourbault & Backeljau, 1997*).

A molecular phylogenetic analysis of the family Draconematidae by *Rho & Min (2011)* revealed that the genus *Dracograllus* was the first lineage to diverge in the family, followed by five branching orders: *Dracograllus—Megadraconema—Draconema—Paradraconema* and *Prochaetosoma*. Consequently, the genus was excluded from the subfamily Draconematinae, as previously suggested. More recently, *Leduc & Zhao (2016)* examined the phylogenetic position of species within Desmodoroidea and confirmed the basal placement of *Dracograllus* within the Draconematidae, consistent with (*Rho & Min, 2011*) findings. Additionally, *Leduc & Zhao (2016)* found that sequences from *Dracograllus*, along with two other specimens of the genus, clustered with high posterior probability and bootstrap support, further reinforcing its basal position in the Draconematidae and providing new insights into the group's evolutionary relationships.

Taxonomic issues. Taxonomic issues within *Dracograllus* include synonymy, redescriptions, and taxon transfers, often arising from descriptions based on immature specimens or discrepancies in the number of longitudinal PAT rows. For example, *Dracograllus eira* was originally described as *Draconema eira* by *Inglis (1968)*, later synonymized with *Dracograllus eira*. Similarly, *Chaetosoma falcatum Irwin-Smith, 1918* underwent multiple reclassifications before being recognized as *Dracograllus falcatus Allen & Noffsinger, 1978*. Another synonym is *Tristicochaeta falcata* Johnston, 1938. Since *Allen & Noffsinger (1978)*, and now, the valid name is *Dracograllus falcatus*. See valid species and nomen nudum section.

Allen & Noffsinger (1978) first described *Dracograllus filipjevi* from holdfasts of kelps from Japan (Oarai, Ibaraki-ken, Honshu Island). It was characterized by: (1) larger body size (500–700 µm long), (2) the absence of cephalic acantiform setae, (3) the presence of longitudinally areolated body cuticle with dot-like punctations, (4) the presence of some cuticular collar in swollen pharyngeal region, and 9 sublateral and 8–9 subventral PAT in males, and 12–13 and 9–10 in females. *Rho, Kim & Kim (2006)* also found *D. filipjev* associated with calcareous algae in Daebo-ri, Guryongpo, Korea, at 3–5 m depth. However, the Korean specimens did not align well with the original description in the number of PATs in male with eight to nine tubes, compared to nine to 11 in the original description. Given that these characteristics are crucial for the taxonomy of Draconematidae, this discrepancy supported the redescription made by *Rho, Kim & Kim (2006)*.

Analyzing the Draconematidae from Guryongpo (Daebo-ri, Korea), *Rho & Min (2011)* reported several species of the genus *Dracograllus*. However, these species are considered invalid, meaning they do not comply with certain taxonomic criteria required for formal recognition (see Article 16.1 of the International Code of Zoological Nomenclature). According to this article, every new name published after 1999 must clearly indicate its new status using specific terms such as 'fam. nov.,' 'gen. nov.,' 'sp. nov.,' 'ssp. nov.,' or an equivalent expression (*e.g.*, 'species nova,' 'new species').

List of valid species.
Dracograllus antillensis Decraemer & Gourbault, 1986
Dracograllus chitwoodi Allen & Noffsinger, 1978

Dracograllus cobbi *Allen & Noffsinger, 1978*

Dracograllus cornutus *Decraemer, 1988*

Dracograllus demani *Allen & Noffsinger, 1978* [*Decraemer, 1988*; *Verschelde & Vincx, 1993*]

Dracograllus eira (*Inglis, 1968*) *Allen & Noffsinger, 1978*; [*Decraemer, 1988*; *Verschelde & Vincx, 1993*]

    Syn. *Draconema eira* *Inglis, 1968*

Dracograllus falcatum (*Irwin-Smith, 1918*)

    Syn. *Chaetosoma falcatum* *Irwin-Smith, 1918*

    Syn. *Notochaetosoma falcatum* (*Irwin-Smith, 1918*) *Cobb, 1929*

    Syn. *Drepanonema falcatum* (*Irwin-Smith, 1918*) *Cobb, 1933*

    Syn. *Claparediella falcatum* (*Irwin-Smith, 1918*) *Filipjev, 1934*

    Syn. *Draconema falcatum* (*Irwin-Smith, 1918*) *Kreis, 1938*

    Syn. *Tristicochaeta falcata* (*Irwin-Smith, 1918*) *Johnston, 1938*

    Syn. *Dracograllus filipjevi* *Allen & Noffsinger, 1978*

    Syn. *Dracograllus gerlachi* *Allen & Noffsinger, 1978*

    Syn. *Dracograllus gilbertae* *Verschelde & Vincx, 1993*

Dracograllus grootaerti *Decraemer, 1988*

Dracograllus kreisi *Allen & Noffsinger, 1978*

Dracograllus laingensis *Decraemer, 1988*

Dracograllus mawsoni *Allen & Noffsinger, 1978*

Dracograllus minutus *Decraemer, 1988* [*Gourbault & Decraemer, 1992*]

Dracograllus miguelitus **sp. nov.** *Johnson da Silva et al., 2025*

Dracograllus ngakei *Leduc & Zhao, 2016*

Dracograllus papuensis *Decraemer, 1988*

Dracograllus pusillus *Decraemer, 1988*

Dracograllus solidus (*Gerlach, 1952*) *Allen & Noffsinger, 1978*

    Syn. *Draconema solidum* *Gerlach, 1952*

Dracograllus spinosus *Decraemer, 1988*

Dracograllus stekhoveni *Allen & Noffsinger, 1978*

Dracograllus timmi *Allen & Noffsinger, 1978* [*Gourbault & Decraemer, 1992*]

Dracograllus trispinosum (*Allen & Noffsinger, 1978*) *Decraemer, 1988*

Syn. *Dracotoranema trispinosum* *Allen & Noffsinger, 1978*

Dracograllus trukensis *Min et al., 2016*

Dracograllus wieseri *Allen & Noffsinger, 1978*

Nomen nudum.

Dracograllus brevitubulus Rho & Kim, 2011 (unaccepted > nomen nudum)

Dracograllus geomunensis Rho & Kim, 2011 (unaccepted > nomen nudum)

Dracograllus gosanensis Rho & Kim, 2011 (unaccepted > nomen nudum)

Dracograllus jaewani Rho & Kim, 2011 (unaccepted > nomen nudum)

Dracograllus jongmooni Rho & Kim, 2011 (unaccepted > nomen nudum)

Dracograllus sungjooni Rho & Kim, 2011 (unaccepted > nomen nudum)
Dracograllus chiloensis Clasing, 1980 (uncertain > taxon inquirendum)

Description of *Dracograllus miguelitus* sp. nov.
(Table 1; Figs. 2–5; S1–S4)

Type material. All specimens are deposited in the Muséum National d'Histoire Naturelle de Paris, France. Male holotype, two juvenile paratypes and the female paratype in the inventory number MNNH-BN511-I1-L1-B. Two male paratypes and female paratypes in MNHN-BN511-I2-L1-A.

Other material. Other specimens are held in the collection of the Laboratoire Environnement Profond of the Biologie et Ecologie des Ecosystèmes marins Profonds research unit-Ifremer, Plouzané, France.

Etymology. The specific epithet is in honor of 'Pedro Miguel', nephew of the first author.

Type locality and habitat. Lucky Strike vent field-MAR. Samples were collected from a hard substratum covered by a thin layer of volcaniclastic sediment, on a visually inactive vent structure at 1,649 m depth. Environmental conditions exhibited background or slightly higher seawater temperature (*i.e.* 4.8–5.7 °C) and higher pH (*i.e.* 7.8–7.9) than the surrounding deep-sea but the activity was very low compared to active habitats where recorded temperature varied between 5.2 °C to 9.5 °C, reaching a maximum of 22.1 °C, and pH varying from 7.2 to 7.6.

Measurements. Table 1.

Holotype male. Habitus typical for the genus. A total of 612 μm long, swollen anterior body region representing 19% of total length (Figs. 2A, 2C). Amphid elongate loop-shaped with non-equal branch sizes, and with one more ventrally than another, amphideal fovea 7.1 μm (Figs. 2C and 3C). Helmet strongly cuticularized (Fig. 2D), with punctations and granular appearance in the lateral part (Fig. 3A). Annulation without ornamentation along the body, except for the tail tip and helmet, with minute punctations (Figs. 2C, 2H, 3D). Four CATs on the rostrum (22.5–26.0 μm long), arranged dorsally in two transverse rows, all with enlarged bases (Figs 2C, 3A, 3B). Some specimens exhibited depressions resembling CAT insertions; however, none of these depressions contained tubes. The setae in the cephalic region and along the body possess a cuticular collar at their insertion and alternation of short and long setae, this collar is projected outside of the cuticle, as a pedicel setae (PS), with 1.2–2.1 μm long (Figs. 2C, 3A, 3B), also in the paratype male (Fig. 6E). Cephalic and cervical region with eight longitudinal rows of setae on each side, between 26 and 32 μm long, and also some irregular minute setae (6–12 μm long) (Fig. 2C). Slender cervical region without lateral differentiation (Figs. 2C and 3A). Buccal cavity narrow, unarmed (Fig. 2B). Cardia short. Pharynx dumbbell-shaped with a weakly developed isthmus from the muscular posterior large endbulb (Figs. 2D, 3A, 3B). Intestine narrow, mostly cylindrical, with a granular appearance, gradually widening posteriorly and lying dorsally to the reproductive system (Figs. 3B–3D). Reproductive system with a single and

Table 1 Morphometric measurements (µm) of *Dracograllus miguelitus* sp. nov.

Parameter	Males		Females		Juveniles	
	Holotype	Paratypes (*n* = 2)	Paratype	Paratypes (*n* =2)	Paratype J3	Paratype J4
L	612	630–735	765.5	748–788	426.3	514.3
a	10.6	13.7–14.9	11.6	12.0–12.8	14.2	10.1
b	6.9	7.4–7.5	7.3	7.7–8.1	5.7	6.3
c	6.2	6.2–7.0	8.1	8.4	6.4	6.9
c'	4.4	4.7–5	4.5	3.8–4.1	3.9	4.4
Head diam.*	32.4	27.2–33.92	31.1	29.6–34.37	19.3	24.3
Amphid. length	15.5	14.2–15.2	14.4	12.7–13.5	9.2	10
Amphid. width	7.12	6.8–6.9	8.2	7.5–7.9	4	4.1
Amphid./cbd(%)	22.0	20.4–25.0	26.6	25.4–25.5	16.7	20.1
Amphid from ant.	5.04	4.1–5	3.5	3.3–3.7	1.5	1.9
Phar. length	88.5	84.0–99.5	93.3	92–103	75.3	80.6
Phar. bulb diam. (ant.)	21.6	20.3–22.8	24.2	26.1–26.7	20.8	22.5
Phar. bulb diam. (post.)	30	29.3–33.5	36.7	34.1–38.5	24.2	28
Max. body diam. Phar.	57.4	45.7–56.3	58.8	58.4–61.6	40.6	54.3
Max. body diam. Mb	44.9	44.8–49.3	49.9	61.8–70	30.1	41.4
Min. body diam.	11.7	16.5–18.59	20.8	20.1–25	20.2	20.6
Spic. length	50.2	47.1–54.9	–	–	–	–
Gub. Apoph. length	13.6	12.7–14.5	–	–	–	–
abd	22	19.9–22.2	18.3	19.7–22.9	17.1	17.3
T. length	97.2	100.8–105.2	84.2	88.6–94.3	66.6	75.9
Non. ann. T. length	43.0	41.1–44	47.4	46.9–53	36.7	38.5
Non. ann. T. length %	44.2	40.8–41.8	56.3	56–59	50.7	55.2
T. length/abd	4.4	4.7–5.0	4.5	3.8	3.8	4.3
Longest tail setae	48.2	49	47.0	45.1–45.8	42.8	44.6
CATn	4	4	4	4	3	4
CATl	22.5–26.0	23.1–30.7	23.7	23.88–24.73	15.5	21.2
1SlATl	62.5	63.4–68.4	58.9	56.8–58.8	47.4	50.4
SlATn**	10	10–12	13	13	5	7
1SvATl	50.0	53.3–54.3	51.5	50.9–50.2	42	44.3
SvATn**	10	10	13	13	5	7
V. to ant.	–	–	317.1	298.5–302.4	–	–
V. (%)	–	–	41.4	39.9–41.3	–	–
PS length	–	–	5.0–5.9	5.5–6.1		–
V. b. diam.	–	–	65.3	64.7–68.8	–	–

Notes:
J3 and J4, third-and fourth-stage juveniles, respectively. L, body length; *a*, ratio of body length to maximum body width; *b*, ratio of body length to pharynx length; *c*, ratio of body length to tail length; *c'*, ratio of tail length to anal body diameter; Head diam., head diameter*; Amphid. length, amphideal length; Amphid. width, amphideal width; Amphid./cbd (%), percentage of amphideal length relative to the corresponding body diameter; Amphid from ant., distance from amphid to anterior end; Phar. length, pharynx length; Phar. bulb diam. (ant.), anterior pharyngeal bulb diameter; Phar. bulb diam. (post.), posterior pharyngeal bulb diameter; Max. body diam. Phar., maximum body diameter at pharynx level; Max. body diam. Mb, maximum body diameter at mid-body; Min. body diam., minimum body diameter; Spic. length, spicule length (measured along the median line); Gub. Apoph. length, gubernaculum apophysis length; abd, anal body diameter; T. length, tail length; Non. ann. T. length, non-annulated tail tip length; Non. ann. T. length (%), percentage of non-annulated tail relative to total tail length; T. length/abd, ratio of tail length to anal body diameter; CATn, number of cephalic adhesive tubes; CATl, length of cephalic adhesive tubes; 1SlATl, length of first sublateral adhesive tube; SlATn, number of sublateral adhesive tubes**; 1SvATl, length of first subventral adhesive tube; SvATn, number of subventral adhesive tubes**; V. to ant., distance from vulva to anterior end; V. (%), vulva position as percentage of total body length; PS length, paravulvar setae length; V. b. diam., vulvar body diameter.
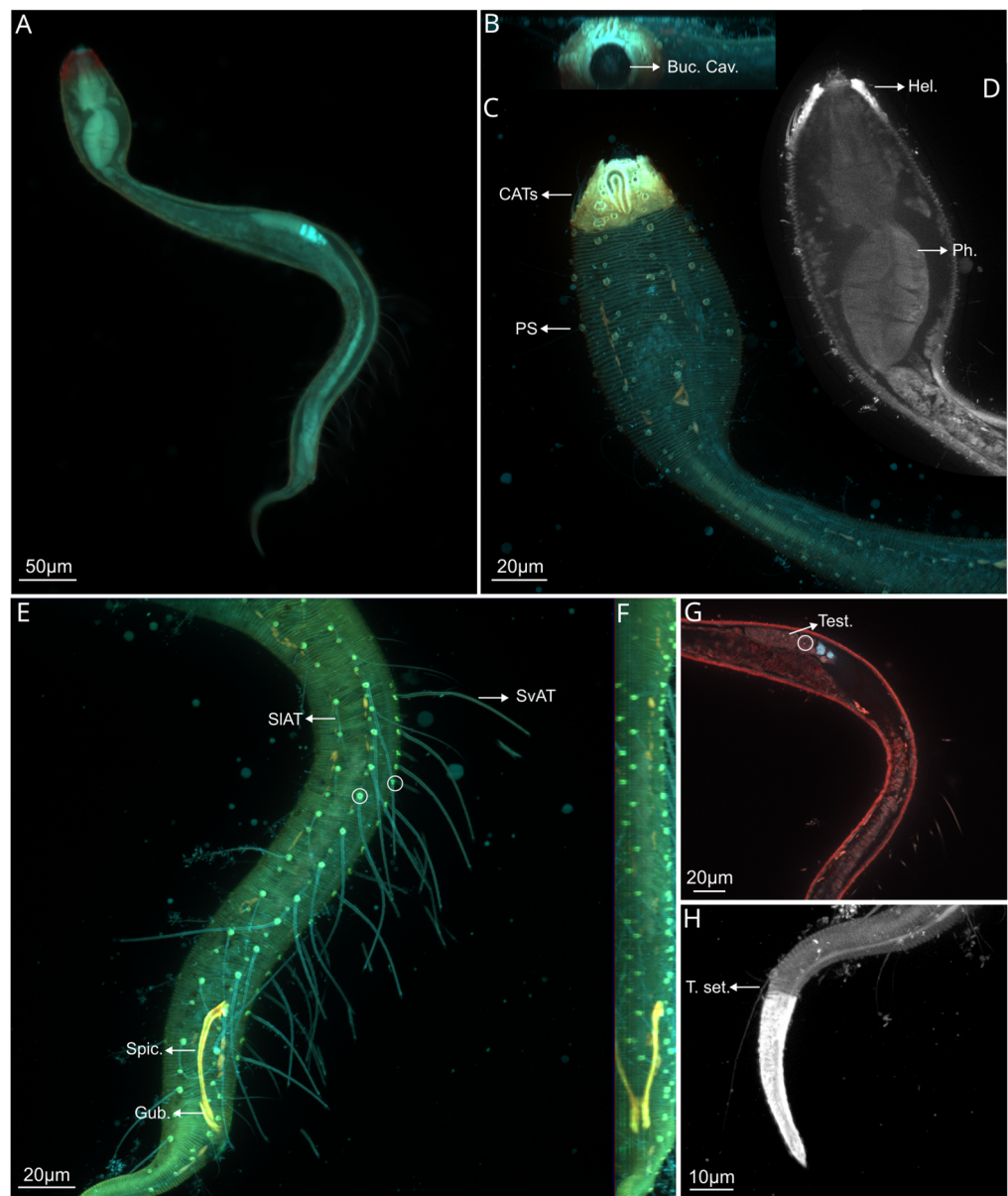* Measured at amphid level.
** In each row.

Figure 2 *Dracograllus miguelitus* sp. nov., 3D fluorescence microscopy. Male holotype. (A) General view (blue, green and red fluorescent channels). (B) Anterior view of the buccal cavity (blue and red fluorescent channels—maximum intensity projection). (C) Swollen anterior region (blue, green and red fluorescent channels—maximum intensity projection), showing the CATs, the amphideal fovea and four of the longitudinal rows of setae and the pedicel setae. (D) Internal view of the head region (blue fluorescent channel—optical section), with the well-cuticularized helmet, some of the CATs and the pharynx. (E) Posterior male region (blue, green and orange fluorescent channels—maximum intensity projection), with both sublateral and subventral rows of PATs, their insertion (circles), spicule and gubernaculum. (F) Ventral view of the posterior regions (blue, green and orange fluorescent channels—maximum intensity projection), with the arcuate spicules. (G) Mid-mody (blue and red fluorescent channels—optical section) showing intestine and testis, circle indicates reproductive cells. (H) Posterior tail region (blue fluorescent channel—maximum intensity projection), with the non-annulated tail region, and the setae associated. Arrows/Abrev: Buc. Cav, buccal cavity; CATS, cephalic adhesive tubes; PS, pedicel setae; Hel, helmet/cephalic capsule; Ph, pharynx; SlAT, sublateral adhesive tubes; SvAT, subventral adhesive tubes; Spic, spicule; Gub, gubernaculum; Test, testis; T. set, tail setae.

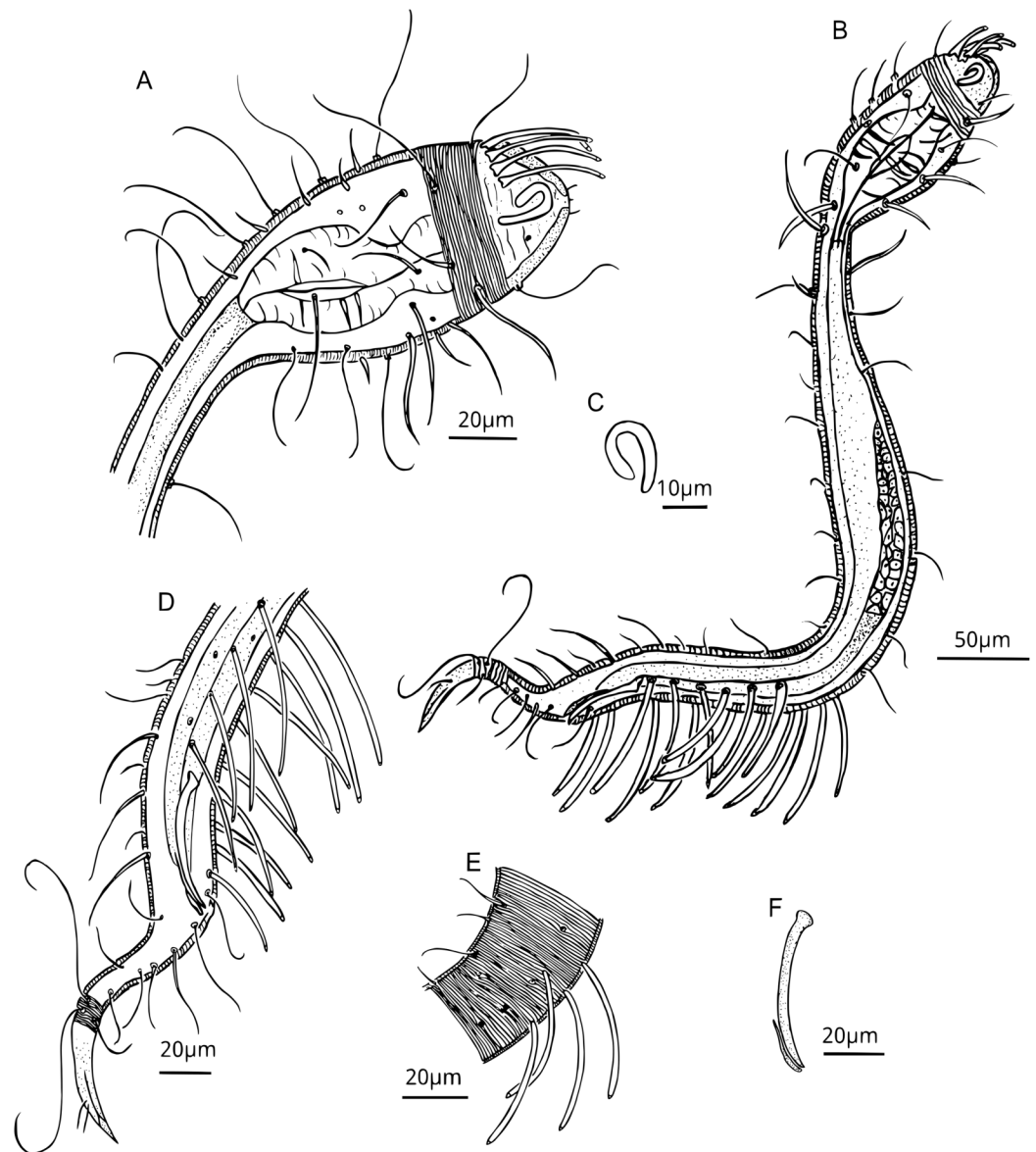Full-size 🖼 DOI: 10.7717/peerj.19585/fig-2

Figure 3 *Dracograllus miguelitus* sp. nov. Male holotype. (A) Head. (B) General view. (C) Fovea. (D) Posterior region, rows of PATs, not all tubes included. (E) Mid-mody curvature, showing the first PATs. (F) Cervical cuticle regions and the three first SvATs and first SlAT, spicule and gubernaculum. Abbrev: PATs, posterior adhesive tubes, SlAT, sublateral adhesive tubes; SvAT, subventral adhesive tubes. Full-size ⬜ DOI: 10.7717/peerj.19585/fig-3

outstretched anterior testis (monorchic) with a well-developed germinative region (Figs. 2G and 3B). Spicules 50.2 μm long, moderately arcuate (in some specimens more arcuate than in others), proximal region with an offset knob-like capitulum (Figs. 2E, 2F and 3F). Gubernaculum 13.6 μm long, lying parallel with the distal end of the spicules, with a minute distal and lateral wing-like expansions (Fig. 3F).

PATs weakly slender, with tongue-like tips (Figs. 2E, 3B, 3D and 3E), difficult to observe due to their thickness. All PATs located anterior to the cloacal opening (Figs. 2E, 3D).
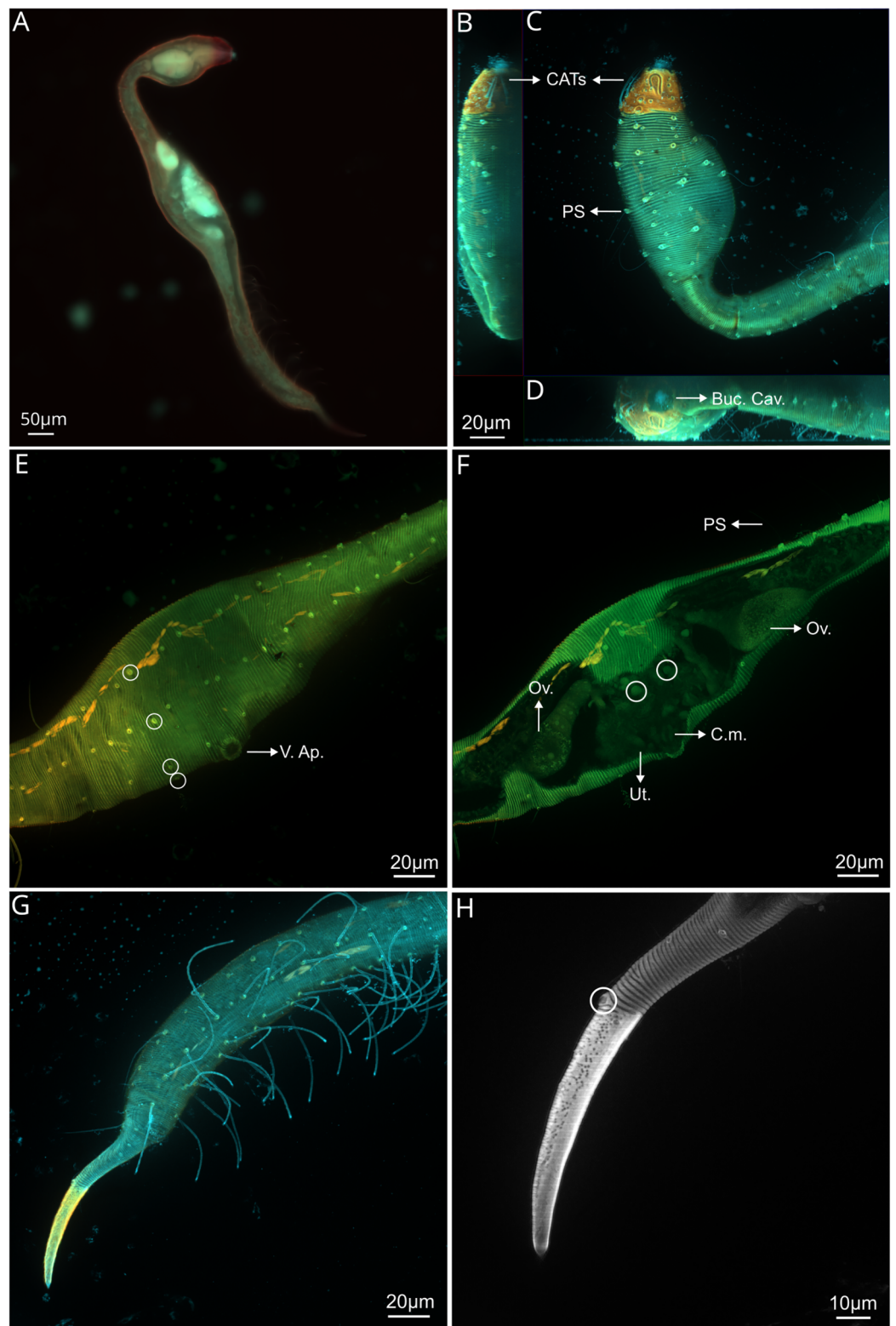
Figure 4 Dracograllus miguelitus sp. nov., 3D fluorescence microscopy. Female paratype.
(A) General view (blue, green and red fluorescent channels. (B) Dorsal view of the head (blue, green and orange fluorescent channels—maximum intensity projection), with the four CATs. (C) Head and cervical region (blue, green and orange fluorescent channels - maximum intensity projection), with evident

Figure 4 (continued)
fovea and pedicel setae, note the clear helmet ornamentation. (D) Face view of the buccal cavity (blue, green and orange fluorescent channels—maximum intensity projection), also CATs and fovea. (E) Mid body region (green and orange fluorescent channels—maximum intensity projection), with the vulvar aperture, and four of the longitudinal rows of setae (circles). (F) Internal view of female reproductive system (green and orange fluorescent channels—maximum intensity projection), reproductive cells within circles. (G) Posterior body region (blue, green and orange fluorescent channels—maximum intensity projection), with some of the both sublateral and subventral rows. (H) Posterior tail region (blue fluorescent channel—maximum intensity projection), with the non-annulated tail region and a setae insertion (circle). Arrows/Abbrev: CATs, cephalic adhesive tubes; PS, pedicel setae; Buc.Cav., buccal cavity; V. Ap., vulvar aperture; Ov., ovaries; Ut., uterus; C.m., constrictor muscles.

Full-size 🖾 DOI: 10.7717/peerj.19585/fig-4

PATs are arranged in four longitudinal rows: two sublateral rows each with 10–12 PATs, and two subventral rows consisting of 10 PATs each one (Figs. 2E, 3D), intermingled setae are present between the PATs. Dorsal posterior part with small and irregular distributed setae between the setae following the rows of the body, more visible than in the ventral side, where only few and minute intermingled setae are present (Figs. 3D). Two pairs of setae are present in the annulated tail region. One pair of long setae in the last annules of the dorsal part of the tail, each setae with a collar at the base, close to each other (48–50 μm long), ventrally, one pair of shorter setae, with collar at the basis (11–12 μm long; Figs 2H, 4B-–4D). Additional five setae are present in the tail, in each somatic row of setae. One to two minute setae in the middle of the non-annulated tail tip (1.5 μm long), in some specimens, some of the setae were absent, but the minute insertion of them is visible.

Paratype female. Similar to males in most aspects, but differ in the following characteristics: greater length, with 765.5 μm long (748–788 μm long in paratypes female and 630–735 μm long in paratypes males; Fig 4A). Amphid also elongated loop-shaped, however slightly wider than in males. In addition, amphid in females is positioned more anteriorly than in males (Figs. 4C, 5B). Pedicel setae at both lateral and ventral side of the head, distributed for all body length and more developed than in males (2.5–3.2 μm long; Figs. 4C, 5B). Swollen pharyngeal region 18% of total body length. Some of the setae appear to be lost, with only the cuticular collars remaining, distributed irregularly and in smaller various sizes than in the head (Figs. 6A, 6B). Just some collars, without setae, are also present in the swollen head region and also on the helmet. Both the anterior and posterior regions of the pharynx vary between sexes. The anterior pharyngeal bulb in females has a diameter of 24–26 μm, and the posterior bulb has a diameter of 34–38 μm (compared to 20–22 μm long and 29–33 μm long respectively in males).

Reproductive system didelphic-amphidelphic with reflexed ovaries, both located ventrally relative to the intestine. Uterus filled with a mass of ovoid reproductive cells (Fig. 4F, circles). The region surrounding the vulvar aperture protrudes outward, with the cuticle giving a labial appearance (Fig. 4E). Two pairs of paravulvar setae present, one anterior and one posterior to the vulvar aperture, with length between 6.09–6.69 μm long. Also a setae emerging from the vulvar aperture (5.03 μm long; Figs. 5A and 5E). Well-developed contractor muscles in the vagina (Fig. 4F). PATs all anterior to the anus,
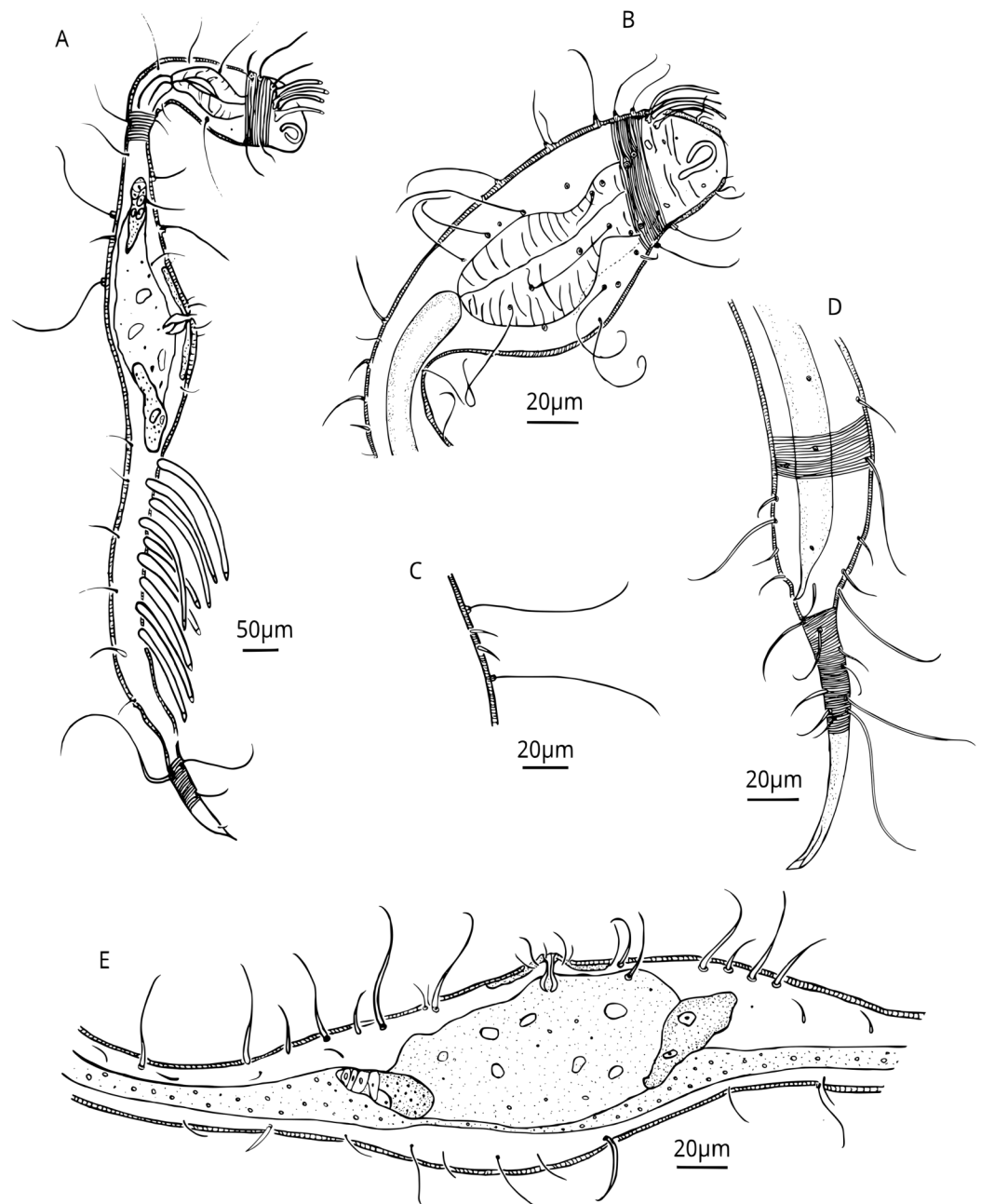
Figure 5 *Dracograllus miguelitus* **sp. nov. Female paratype.** (A) General view; (B) Head. (C) Cuticle at cervical region. (E) Posterior and tail region, female reproductive system.

more slender, but shorter than in males (56.8–58.8 *vs* 63.4–68.4 in males), with weakly developed bell shaped tips with a tongue-like valve. PATs arranged in four longitudinal rows: two sublateral rows each consisting of 13 adhesion tubes with intermingling and irregular somatic setae and two subventral rows of 13 adhesion adhesion tubes also with intermingling somatic setae (Fig. 4G). First SlAT on the females with 58.9 μm long and
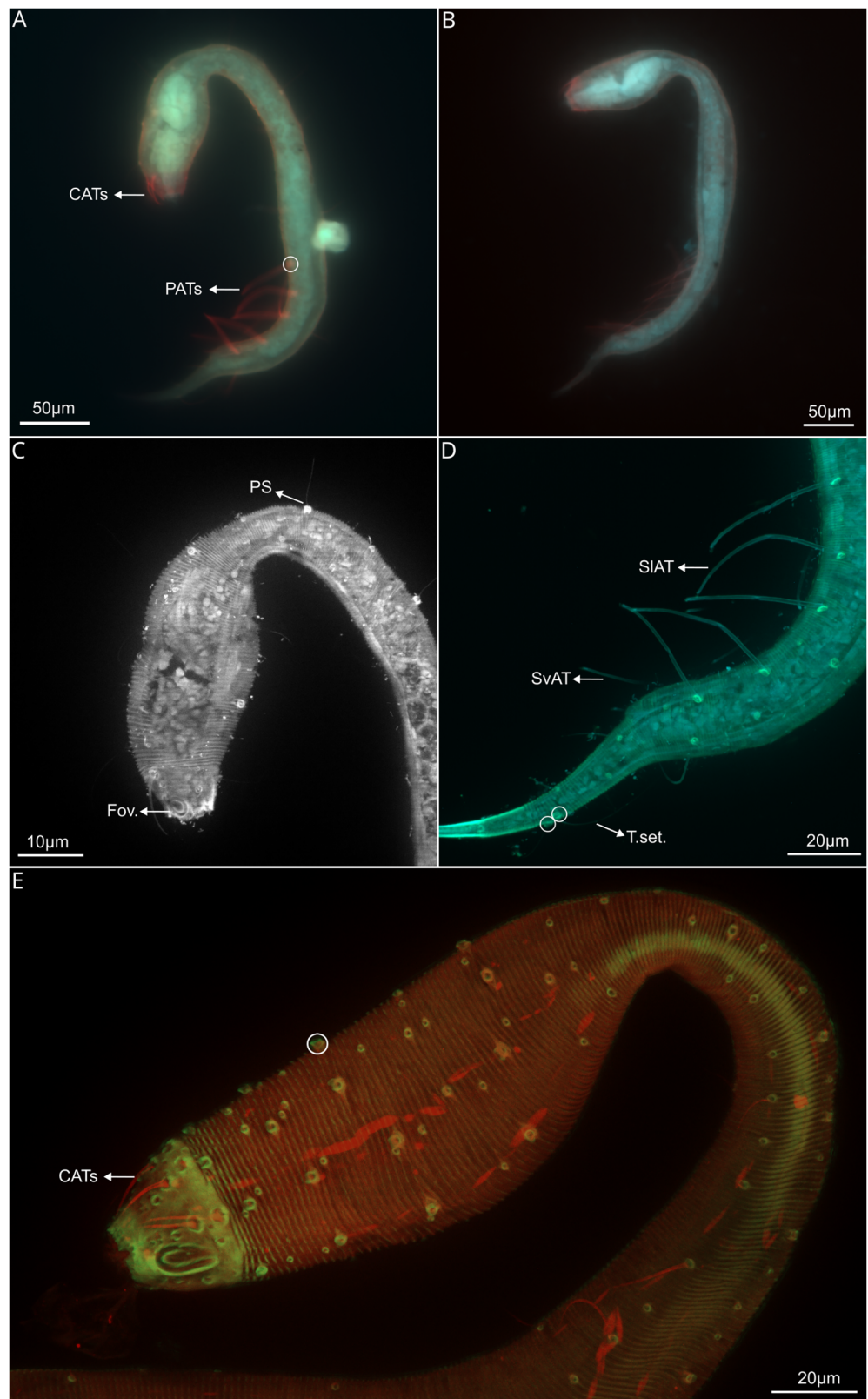
Figure 6 *Dracograllus miguelitus* sp. nov., 3D fluorescence microscopy of the juveniles and a male paratype. (A) General view of juvenile third stage (blue, green and red fluorescent channels), showing

Johnson da Silva et al. (2025), *PeerJ*, DOI 10.7717/peerj.19585

17/45

62.5 on males. All PATs weakly broadened at insertion base. Tail gradually tapering posteriorly to a cylindro-conoidal non-annulated tail tip (Figs. 4H, 5A and 5D). One pair of long setae in the last annules of the dorsal part of the tail (Figs. 4H, circle and 5D). Each setae with a collar at the base and close to each other (50.44 μm long). Ventrally, there is one pair of short setae with also a collar at the base (11–13 μm long). Two pairs of setae are present on the last annules of the tail, each setae featuring a collar at its base and positioned close to one another, measuring 52–56 μm in length (Fig. 5D). Additionally, there is another pair of shorter setae, also with collars at their bases, measuring 12–14 μm in length (Figs. 4G, 4H, 5D). Five more setae are distributed along the tail, in similar size as in males, in each somatic row of setae. One or two minute setae (1.5 μm long) are located at the non-annulated tail tip. In some specimens, one of these setae (and also for those on the annulated tail) is absent, though its minute insertion point remains visible (Fig. 4H). Non-annulated tail tips are long, constituting 56–59% of total tail length. Caudal glands not evident.

Juveniles paratypes

Juvenile third stage. Body shape similar to adults. Body length 426.3 μm long, head diameter 19.3 μm long and a pharynx 75.3 μm long, with a minimally developed isthmus (Fig. 6A). Swollen region representing 24% of the total length. Amphideal fovea is smaller in both length (9.2 μm) and width (4 μm), circular and closed-shape (Fig. 6C). Several pedicel setae with 2.18 μm long, in some specimens as long as in some in adults (Fig. 6C). Two CATs in the dorsal region of the helmet, all at the level of the amphid (15.89–22.24 μm long) (Fig. 6C). Five PATs in both subventral and sublateral row (Figs. 6A, 6D). Tail slender, with the non-annulated tail tip corresponding to 50.7% of the tail length, similar to that in adults (Fig. 6D). The cuticle of the non-annulated tail tip end ornamented with minute punctations. All observed juveniles exhibit a globular appearance on the lateral sides of the body between the body wall and the cuticle, sometimes with brownish or yellowish coloration in the pharyngeal and anterior region.

Juvenile fourth stage. Body shape similar to adults. Body length 514.3 μm long, with head diameter 24.3 μm long. Swollen region representing 25.2% of the total length (Fig. 6B). Amphideal fovea 80.6 μm, circular and closed, similar to the third stage. Presence of pedicel setae with 2.82 μm long. Three CATs located on the helmet with the longer one and

more evident with 21.2 μm long. Seven PATs on both sublateral and subventral row, first SlAT with 50.4 μm long and first SvAT with 44.3 μm long (Fig. 6B).

Diagnosis.

D. miguelitus **sp. nov.** is characterized by the presence of four CATs located in the dorsal side of the helmet at the level of the amphid. All CATs situated anterior to the cuticular annulations. Amphid elongate loop-shaped with different branch sizes in males and females and circular in juveniles. A collar is present at the base of some setae, as a pedicel-like structures. Paravulvar setae are present in two pairs, one anterior and one posterior to the vulvar aperture. Additionally, a minute setae is visible parallel to the vulvar aperture. In the males, PATs are arranged in four longitudinal rows: two sublateral rows each with 10–12 CATs, and two subventral rows consisting of 10 PATs each one. In the females, sublateral and subventral rows with 13 CATs each one. Two pairs of setae in the annulated part of the tail, one pair with long setae (40–50 μm and one pair with shorter setae (11–13 μm). The non-annulated tail tip corresponds to 40–44% in males, 56–59% in females, and 50–55% in juveniles.

Differential diagnosis and relationship

Dracograllus miguelitus **sp. nov.** is immediately distinguished from its congeners by possessing only four cephalic adhesive tubes (CATs) located at the level of the amphid, in contrast to species with six CATs (*D. minutus*), eight CATs (*D. antillensis, D. chitwoodi, D. cobbi, D. demani, D. eira, D. filipjevi, D. gilbertae, D. grootaerti, D. kreisi, D. laingensis, D. mawsoni, D. ngakei, D. papuensis, D. pusillus, D. solidus, D. spinosus, D. timmi, D. trispinosum, D. trukensis*, and *D. wieseri*), or more, such as *D. cornutus* (11 CATs), *D. falcatus* (12 CATs), *D. gerlachi* (13 CATs), and *D. stekhoveni* (14 CATs).

The absence of cuticular ornamentation further differentiates *D. miguelitus* **sp. nov.** from species with spines (*D. antillensis, D. chitwoodi, D. grootaerti, D. minutus*, and *D. trukensis*) or dot-like punctations (*D. filipjevi, D. gerlachi, D. kreisi, D. pusillus*, and *D. trispinosum*). The cuticle of *D. miguelitus* **sp. nov.**, with the collars at the bases of its setae, resembles those observed in *D. cobbi, D. mawsoni, D. filipjevi*, and *D. timmi*, though the setae in these species are significantly smaller compared to those in *D. miguelitus*. The presence of paravulvar setae distinguishes *D. miguelitus* **sp. nov.** from several species, including *D. chitwoodi, D. cobbi, D. cornutus, D. filipjevi, D. grootaerti, D. minutus, D. ngakei, D. pusillus, D. solidus, D. spinosus, D. stekhoveni, D. timmi, D. trispinosum*, and *D. trukensis*, all of them lacking setae at the vulva.

Dracograllus miguelitus **sp. nov.** is geographically closest to *D. demani* and *D. trispinosum* but can be distinguished from these species by several morphological features. See Tables 2 and 3 for the morphometrical and descriptive comparison between all the valid species In addition to the number of cephalic adhesive tubes (CATs)—four in *D. miguelitus* **sp. nov.** compared to eight in both *D. demani* and *D. trispinosum*—the new species differs in the number of sublateral adhesive tubes (10–12 in *D. miguelitus* **sp. nov.** *vs* six in *D. demani* and 10 in *D. trispinosum*), subventral adhesive tubes (10 in both *D. miguelitus* **sp. nov.** and

Table 2 Morphometrical comparison for all valid species of *Dracograllus* genus including *Dracograllus miguelitus* sp. nov.

Species	L	CATn	SlATn	SvATn	Spicule	Non-annulated tail tip %
D. antillensis Decraemer & Gourbault, 1986	Ms: 410–510	8	Ms: 6–10	Ms: 9–14	36–40	Ms:14–20
	Fs: 410–510		Fs: 7–9	Fs: 8–12		Fs: 29–32
D. chitwoodi Allen & Noffsinger, 1978	Fs:500–600	8	Fs: 9–10	Fs: 8–10	–	Fs: 50–54
D. cobbi Allen & Noffsinger, 1978	M:500	8	M: 9	M: 12	51	M: 44
	F: 500		F: 8	F: 14		F: 53
D. cornutus Decraemer, 1988	Ms: 495–610	10–11	Ms: 16	Ms: 13	55–56	Ms: 26–28
	Ms: 480		Ms: 18	Ms: 16		Ms: 49
D. demani Allen & Noffsinger, 1978	Ms: 500–800	8	Ms: 5–7	Ms: 8–12	45–53	Ms: 24–39
	Fs: 500–800		Fs: 6–8	Fs: 10–13		Fs: 41–51
D. eira (Inglis, 1968)	M: 500	8	M: 12	M: 8	48	M: 48
	F: 600		Fs: 12	Fs: 8		F: 41
D. falcatus (Irwin-Smith, 1918)	M: 800	12	M: 12	M: 17	71	M: 32
	F: 900		F: 21	F: 23		F: 48
D. filipjevi Allen & Noffsinger, 1978	Ms: 500–700	8	Ms: 8–11	Ms: 9–11	37–40	Ms: 40–50
	Fs: 600–700		Fs: 12–14	Fs: 9–11		Fs: 46–55
D. gerlachi Allen & Noffsinger, 1978	M: 600	13	M: 13	M: 18	39	M: 28
	F: 700		F: 24	F: 21		F: 28
D. gilbertae Verschelde & Vincx, 1993	M: 581	8	M: 10	M: 9	59	M: 20
	F: 639		F: 13	F: 10		F: 42
D. grootarti Decraemer, 1988	M: 650	8	M: 10	M: 14	68	M: 46
	Fs: 675–755		Fs: 12–13	Fs: 7–9		Fs: 43–61
D. kreisi Allen & Noffsinger, 1978	M: 400	8	M: 5	M: 11	36	M: 40
	F: 400		F: 12	F: 9		F: 69
D. laingensis Decraemer, 1988	M: 460	8	M: 8–9	M: 8	39	M: 24
	F: 440		F: 5	F: 5		F: 43
D. mawsoni Allen & Noffsinger, 1978	Ms: 500–600	8	Ms: 13	Ms: 13	52–54	Ms: 28–35
	F: 700		F: 15	F: 16		F: 58
D.miguelitus sp. nov.	Ms: 630–735	4	Ms: 10–12	Ms: 10	47–54	Ms: 40–41
	Fs: 748–788		Fs: 13	Fs: 13		Fs: 56–59
D. minutus Decraemer, 1988	M: 290	6	M: 5	M: 2–3	18	M: 24
D. ngakei Leduc & Zhao, 2016	M: 576	8	M: 11	M: 10	50	M: 28
	Fs: 586–615		Fs: 13	Fs: 10–12		Fs: 37–50
D. papuensis Decraemer, 1988	M: 310	8	M: 10	M: 11	29	M: 75
	Ms: 350–400		Ms: 9–11	Ms: 9–11		Ms: 46–56
D. pusillus Decraemer, 1988	M: 310	8	M: 10	M: 6	26	M: 28%
D. solidus (Gerlach, 1952)	M: 700	8	M: 7	M: 11	46	M: 29
	Fs: 600–800		Fs: 8–11	Fs: 8–11		Fs: 46
D. spinosus Decraemer, 1988	M: 340	8	M: 8	M: 10	45	M: 49%
D. stekhoveni Allen & Noffsinger, 1978	Ms: 500–600	14	Ms: 16–23	Ms: 16–23	40–50	Ms: 22–34
	Fs: 500–600		Fs: 20–25	Fs: 21–29		Fs: 37–47

Table 2 (continued)						
Species	L	CATn	SlATn	SvATn	Spicule	Non-annulated tail tip %
D. timmi *Allen & Noffsinger, 1978*	Ms: 500–700	8	Ms: 7–10	Ms: 19–23	41–51	Ms: 29–36
	Fs: 500–600		Fs: 9–12	Fs: 7–11		Fs: 43–52
D. trispinosus (*Allen & Noffsinger, 1978*)	Ms: 700	8	Ms: 10	Ms: 6–7	59–64	Ms: 26–27
	Fs: 600–800		Fs: 12–13	Fs: 8–13		Fs: 52–61
D. trukensis Min et al., 2016	Ms: 593–642	8	Ms: 10	Ms: 8–10	34–42	Ms: 43–48
	Fs: 663–778		Fs: 13–15	Fs: 9–11		Fs: 45–58
D. wieseri *Allen & Noffsinger, 1978*	M: 600	8	M: 17	M: 13	46	M: 26
	F: 500		F: 14	F: 12		F: 45

Note:
L, body length; CATn, number of cephalic adhesive tubes; SlATn, number of sublateral adhesive tubes; SvATn, number of subventral adhesive tubes; Ms, type series males; M, male holotype; Fs, type series females; F, female holotype. L and spicule measurements expressed in μm.

D. demani, but seven in *D. trispinosum*), and spicule length (50 μm in *D. miguelitus* sp. nov., compared to 37 μm in *D. demani* and 61 μm in *D. trispinosum*). Additionally, the non-annulated tail tip of *D. miguelitus* **sp. nov.** is longer (44% of body length in the male holotype and 56% in the female paratype) compared to the shorter tail tips in *D. demani* and *D. trispinosum* (32% and 26%, respectively). Morphometrical and descriptive comparison between all the valid species (Tables 2 and 3).

Comments on the imaging approach

Several challenges related to the study of marine nematodes have been discussed here, and we would like to emphasize one of the most important ones: the difficulty in observing and measuring their morphological structures. Therefore, it is crucial to investigate advanced imaging methods to facilitate identification and capture additional morphological features (*Foulon, Malloci & Zeppilli, 2025* in press). The pioneering work of *Zullini & Villa (2009)* first documented the autofluorescence using confocal microscopy of free-living nematodes, with the redescription of *Eutobrilus andrassyi*. Other examples include the redescriptions of *Craspodema reflectans* (Cyatholaimidae) and *Longicyatholaimus maldivarum* (Cyatholaimidae) by *Semprucci & Burattini (2015)* and *Semprucci et al. (2017)*, respectively. Additionally, an introduction to the application of confocal techniques for observing marine nematodes is provided in *Semprucci et al. (2016)*. In our study, 3D fluorescence imaging has proven effective in several key aspects of identification, particularly for the Draconematidae family. We observed that various structures, that are difficult to study with traditional microscopic techniques, were analyzed with relative ease in our study. These included the insertion of the CATs, the cuticular ornamentation or annulations, and the number of rows of setae. Videos of the 3D fluorescence captures and additional pictures are available in the Supplemental Material (S1–S4).

Biodiversity, distribution and ecology

In terms of species diversity, *Dracograllus* is the largest genus in the Draconematidae family, with 26 valid species (*Nemys, 2024*). These species are distributed across a variety of marine environments, and despite their large distribution, the genus is predominantly

Table 3 Descriptive comparison for all valid species of *Dracograllus* genus including *Dracograllus miguelitus* sp. nov.

Specie	Ann. Ornam.	Fov. M.	Fov. F.	PS	Anal flap	Diff. Diagnosis
D. antillensis	Spine-like	Large, conspicuously 'U'-shape with ventral arm often slightly longer than dorsal	–	–	Absent	Spicules 35–40 µm long, arcuated and cephalated. Gubernaculum 11–15 µm long, with *corpus* and lateral wind. Four long somatic setae between the eighteenth SlATs.
D. chitwoodi	Spine-like	–	Elongated loop-shape	Absent	Present. short	Fewer SlATs and SvATs, absence of PS, and setae without collar at the base.
D. cobbi	Without	Elongated loop-shape	Elongated loop-shape	One pair anterior to the vulva (6–7 µm long)	Absent	Great number of SlATs in males, shorter caudal glands and anterior position of the vulva.
D. cornutus	Without	Short loop-shape	Short loop-shape	Absent	Absent	Similar to Dracotoramonema *Allen & Noffsinger, 1978*, but cornifor setae and length of SlATs less conspicuous than in *Dracotoramonema trispinosum*
D. demani	Without	Elongated loop-shape	Elongated loop-shape	Two setae (7–9 µm long)	Absent	PS in ventro-sublateral rows, but only anterior to the SlATs.
D. eira	Without	Elongated loop-shape	Elongated loop-shape	Absent	Absent	All CATs anterior to the amphid, and 1 SlAT on the non-annulated tail region. Males with SlATs posterior to the anus.
D. falcatum	Without	Elongated loop-shape	Elongated loop-shape	Two pairs, one anterior and one posterior to the vulva	Absent	Rostrum without Ceph Acan-set and with 12 CATs
D. filipjevi	Dot-like	Elongated loop-shape	Elongated loop-shape	Two pairs, one anterior and one posterior to the vulva. (5–6 µm long)	Absent	Scattered minute spiny on cuticle, Absence of PS.
D. gerlachi	Dot-like punctations, more evident at mid-body	Elongated loop-shape	Elongated loop-shape	Two pairs, one anterior and one posterior	Absent	13 CATs on rostrum and great swollen esophageal region
D. gilbertae	Broad interannual space, ornamented with a slit	Large, ventrally whorled, open loop-shape	Large, closed loop-shaped	Absent	Absent	Large amphideal fovea, long and slender PATs. Slender tail with ventral post cloacalpostcloacal swelling. Spicules long and well cuticularized gubernaculum.
D. grootaerti	Spine-like	Long, inverted U-shaped, with longer ventral arm extending to the first annule	As in male, but shorter	Absent	Absent	Long body, with spiny ornamentaded annulated cuticle. Two of the SlATs in females on the tail region.

Table 3 (continued)

Specie	Ann. Ornam.	Fov. M.	Fov. F.	PS	Anal flap	Diff. Diagnosis
D. kreisi	Dot-like punctations	Elongated loop-shape	Elongated loop-shape	Absent	Absent	Absence of PS in ventro-sublateral row and shorter spicules in males.
D. laingensis	Spine-like	Long, inverted U-shaped	Elongated unispiral	Absent	Absent	Long swollen pharyngeal regions, and stiff posteriorly directed setae anterior to PATs.
D. mawsoni	Without	Elongated loop-shape	Slightly smaller, with more open loop than in male	Two pairs, one anterior and one posterior to the vulva. (4–7 µm long)	Absent	Great number of SlATs in males, and females with 1 SlAT posterior to anus
D. miguelitus sp. nov.	Without	Elongated loop-shaped, ventrally coiled, ventral arm slightly longer	Inverted U-shaped with branches more equal in size and more closed than in males	Two pairs, one anterior and one posterior to the vulva (6 µm long). Single seta emerging from the vulvar aperture	Absent	4 CATs on the rostrum, PS longer in males than in females.
D. minutus	Spine-like	Very large, loop-shape, ventrally whirled	–	–	Absent	Smaller body size within the genus, only six CATs on rostrum, short spicules. Largest fovea within the genus.
D. ngakei	Without	Loop-shaped, with two arms of equal length	Loop-shaped, with two arms of equal length	Absent	Absent	11 SvATs per row in male, all anterior to anus. Females with 12 SvATs with one of themn posterior to anus.
D. papuensis	Finely annulated	Long, inverted U-shaped, ventrally coiled, ventral arm slightly longer	Large, loop-shaped. dorsal arm slightly longer than ventral one	Minute setae: two ventral posterior and one anterior to the vulva	Absent	Shorter swollen pharyngeal region, spicule and c-value.
D. pusillus	Dot-like punctations at ring edges in the pharyngeal region	Long, inverted U-shaped. ventrally coiled, ventral arm slightly longer	–	–	Absent	Short and stout body with minute spiny ornamentations, short spicule. Long non-annulated tail tip.
D. solidus	Without	Elongated loop-shape	Elongated unispiral	Absent	Absent	11 long setae intermingled with SlATs in males, unispiral amphid and 2 SlATs posterior to anus in females.
D. spinosus	Without	Large, oblique loop-shape by position of sublateral CAT, ventrally whirled; Ventral arm slightly longer than dorsal arm	–	–	Absent	Spiny ornamentation at the insertion base of several somatic setae in the posterior body region. Females and juveniles not found.

(Continued)

Table 3 (continued)

Specie	Ann. Ornam.	Fov. M.	Fov. F.	PS	Anal flap	Diff. Diagnosis
D. stekhoveni	Without	Elongated loop-shape	Elongated loop-shape	Two pairs, one anterior and one posterior to the vulva. (3–5 μm long)	Absent	1 pair of sub-lateral cephalic acant setae on rostrum.
D. timmi	Spine-like projections	Elongated loop-shape, some specimens ventral arm curved anteriorly toward dorsal arm almost forming unispiral	Elongated loop-shape	Two pairs, one anterior and one posterior to the vulva. (5–7 μm long)	Absent	Faint annular ridges with spine-like projections appearing as 2 rows of fine punctations.
D. trispinosum	Dot-like punctations	Very large, loop-shape	Elongated unispiral	–	Absent	Males with 3 large Corn-set, a single ventral mid-body setae and 1 preanal pair.
D. trukensis	Ridges with spiny protrusion, spiny ornamentation	Large. Elongated, open loop-shaped, longer ventral arm extending to the first body cuticular annule	Large, elongated and closed loop-shaped, shorter than in male	Absent	Absent	Numerous minute spiny ornamentation on male and female cuticle. Shorter spicule in males.
D. wieseri	Granules and vacuoles	Elongate loop-shape	Elongate loop-shape	Absent	Present. Short	6 long setae intermingled with SlATs in males, and SlAT 1 in females posterior to anus.

Note:
Ann. Ornam., annules ornamentation; Fov. M., amphideal fovea male; Fov., amphideal fovea female; Parav. set., paravalvular setae; "–": not provided in the original description or not applicable.

associated with shallow, tropical and subtropical regions (*Min et al., 2016*). The distribution and general ecological characteristics of all *Dracograllus* valid species are presented in Table 4. The *Dracograllus* genus includes species distributed across the Pacific (18 species), Atlantic (nine species) and Indian (four species) oceans. Some species, such as *D. eira*, occur in multiple oceanic regions, underscoring their adaptability to diverse oceanic regimes. Distribution of all valid species, and species occurrences including non-identified *Dracograllus* specimens are provided in Fig. 7. The Pacific Ocean is the region where the highest number of *Dracograllus* species have been both recorded and described, likely reflecting a bias due to a more extensive sampling. Examples *include D. cornutus, D. falcatus, D. filipjevi, D. gerlachi, D. grootaert, D. laingensis, D. mawsoni, D. minutus, D. papuensis, D. pusillus, D. spinosus, D. timmi, D. trukensis*, and *D. wieseri* from a variety of habitats and environmental conditions, particularly in coastal regions. More recently, *Leduc & Zhao (2016)* described *D. ngakei*, a species from intertidal coarse sand and gravel sediments in New Zealand, including molecular and morphological data.

In the Atlantic Ocean, species such as *D. antillensis, D. chitwoodi*, and *D. kreisi* are typically found in shallow marine environments, often associated with sandy beaches on intertidal or subtidal zones. *Decraemer & Gourbault (1986)* found approximately 500 individuals of *D. antillensis* in samples from Guadeloupe, a notably high number for a single species, especially when compared to the abundances typically observed in

Table 4 Distribution and ecological characteristics of *Dracograllus* species.

Species/reference	Ocean	Geographic distribution	Habitat	Habitat type, sampling and conditions	Remarks
D. antillensis Decraemer & Gourbault, 1986; Stock & Nadler, 1998*	Atlantic	Guadeloupe Island: Anse de la Gourde, Grande Terre; Les Galets, Capesterre; Petite Anse, La Marie-Galante. Martinique Island: Anse l'Étang; Anse Figuiers.	Intertidal region	Sandy beach; interstitial waters with coarse and calcareous sediments.	–
*D. chitwoodi Allen & Noffsinger, 1978**	Atlantic	Coral Key, Florida, USA	Subtidal region	Sandy beach; sediment associated with calcareous algae (*Halimeda sp.*).	Males only measured, without complete description. No third or fourth-stage juvenile observed.
D. cobbi Allen & Noffsinger, 1978; Decraemer, 1988.*	Atlantic	Coral Key, Florida, USA; Anse de la Gourpe, Guadeloupe.	Intertidal region	Sandy beach; sediment associated with calcareous algae (*Halimeda sp.*).	Females from Guadeloupe lack paravalvular setae and show other differences compared to the original description. See *Decraemer, 1988*.
*D. cornutus Decraemer, 1988**	Pacific	Laing Island, Papua New Guinea and River Mouth, NT, Australia	Subtidal region	Sandy beach; sediment sampling	-
D. demani Allen & Noffsinger, 1978; Decraemer, 1988; Verschelde & Vincx, 1993; Shahina et al., 2019*	Atlantic, Pacific and Indian	Marseille, France; Laing Island, Duangit Reef, Papua New Guinea; Malindi, Kenya; Pakistan.	Subtidal region, down to 42 m depth	Sandy beach; coarse sand with algae and coarse coral sand	Specimens from Papua New Guinea differ from the type locality by having a shorter general body length, shorter PATs, and shorter spicules.
D. eira Inglis, 1968; Decraemer, 1988; Verschelde & Vincx, 1993*	Pacific and Indian	St. Vincent's Bay, New Caledonia; Laing Island, Papua New Guinea; Malindi, Kenya	Subtidal and intertidal zone	Sediments associated with polychaete tubes and large pieces of dead coral.	–
D. falcatus Irwin-Smith, 1918; Allen & Noffsinger, 1978*	Pacific	Cremorne, Port Jackson, New South Wales, Australia; Long Reef and Vaucluse, Australia	Subtidal region, from 1.2 - 1.5 m depth	Sandy beach; sediment sampling with seaweed and shells	–
D. filipjevi Allen & Noffsinger, 1978; Rho, Kim & Kim, 2006*	Pacific	Oarai, Ibaraki-ken, Honshu Island, Japan; Daebo-ri, Guryongpo, Korea	Subtidal region	Washings of holdfasts of Kelps and also in shallow littoral calcareous algae	–
D. gerlachi Allen & Noffsinger, 1978; de Jesús-Navarrete*	Atlantic and Pacific	Ibusuki, Kyushu Island, Japan and Laguna de Términos, Gulf of Mexico	Subtidal region	Sandy beach; sediment sampling with brown algae growing on rocks	–
*D. gilbertae Verschelde & Vincx, 1993**	Indian	Gazi, Kenya	Subtidal region	Sandy beach; core of 3.5 cm diameter into the sediment down to 20 cm depth, close to mangrove plants (*Sonneratia* sp.)	–
*D. grootaerti Decraemer, 1988**	Pacific	Madang Province, Hansa Bay, Duangit Reef, Laing Island, Papua New Guinea	Subtidal region at 42 m depth.	Sandy beach; sediment sampling with polychaete tubes, and coral sand	–

(Continued)

Table 4 (continued)

Species/reference	Ocean	Geographic distribution	Habitat	Habitat type, sampling and conditions	Remarks
*D. kreisi Allen & Noffsinger, 1978**	Atlantic	Coco Solo, on Galeta Beach, Panama	Subtidal region	Sediment associated with calcareous algae (*Halimeda sp.*).	–
*D. laingensis Decraemer, 1988**	Pacific	Laing Island, Papua New Guinea	Subtidal region at 42 m depth.	Sediment sampling with polychaete tubes, and coral sand	–
*D. mawsoni Allen & Noffsinger, 1978**	Pacific	Long Nose Point, Port Jackson, New South Wales, Australia	Subtidal region	Sandy beach; sediment sampling with bottom debris	–
*D. minutus Decraemer, 1988**	Pacific	Laing Island, Papua New Guinea	Subtidal region	Sediment sampling with polychaetes tubes of sand and mucus	No female or juvenile known
D. miguelitus sp. nov. Johnson et al., 2024*	Atlantic	Lucky Strike vent field, Mid Atlantic Ridge	Deep-sea	Hydrothermal inactive vent structure;	Only present in the inactive vent structure at LS, without individuals in active or periphery samples.
*D. ngakei Leduc & Zhao, 2016**	Pacific	Hataitai Beach, Wellington, New Zealand	Mid-intertidal region	Sandy beach; sediment sampling (0 to 10 cm sediment depth) with coarse sand and gravel	SSU Molecular sequences available in original description.
*D. papuensis Decraemer, 1988**	Pacific	Laing Island, Papua New Guinea	Subtidal region	Sediment sampling with dead coral debris, also with polychaete tubes of sand and mucus	Only one male found, without non-annulated tail tip length known.
*D. pusillus Decraemer, 1988**	Pacific	Laing Island, Papua New Guinea	Subtidal region	Sediment sampling, with dead coral debris	–
*D. solidus Gerlach, 1952**	Atlantic and Indian	Banyuls, France; Bay of Biscay, Mediterranean sea; Mascarene Islands.	Subtidal region	Sandy beach; sediment sampling	Also recorded in Mascarene Islands, no juvenile known.
*D. spinosus Decraemer, 1988**	Pacific	Laing Island, Papua New Guinea	Subtidal region	Sediment sampling with polychaete tubes, sand and mucus	Males and juveniles not found.
D. stekhoveni Allen & Noffsinger, 1988*	Pacific	Solano, Colombia; Port Jackson, Australia; Isla Taboga, Panama	Subtidal region	Sandy beach; sediment sampling with corals	Juveniles specimens third stage without PS.
*D. timmi Allen & Noffsinger, 1978**	Pacific	Bora Bora Island, Society Islands	Subtidal region	Sandy beach; sediment sampling of coarse sand	Second and third-stage juveniles not found
*D. trispinosus Allen & Noffsinger, 1978**	Atlantic	Southwest of the Pomegues Ratonneau jetty, near Marseille, France	Subtidal region	Sandy beach; sediment sampling at 20 m depth.	–
*D. trukensis Min et al., 2016**	Pacific	Weno, Chuuk, Micronesia	Subtidal region	Sandy beach; sediment sampling with seagrass bed (*Zostera* sp., from 1 to 2 m depth)	–
*D. wieseri Allen & Noffsinger, 1978**	Pacific	Juan Fernandez Islands, Chile	Subtidal region during high tide zone	Sandy beach; sediment sampling with green algae	–

Note:
References marked with an asterisk (*) indicate the original description and type locality, while those without an asterisk refer to additional localities.
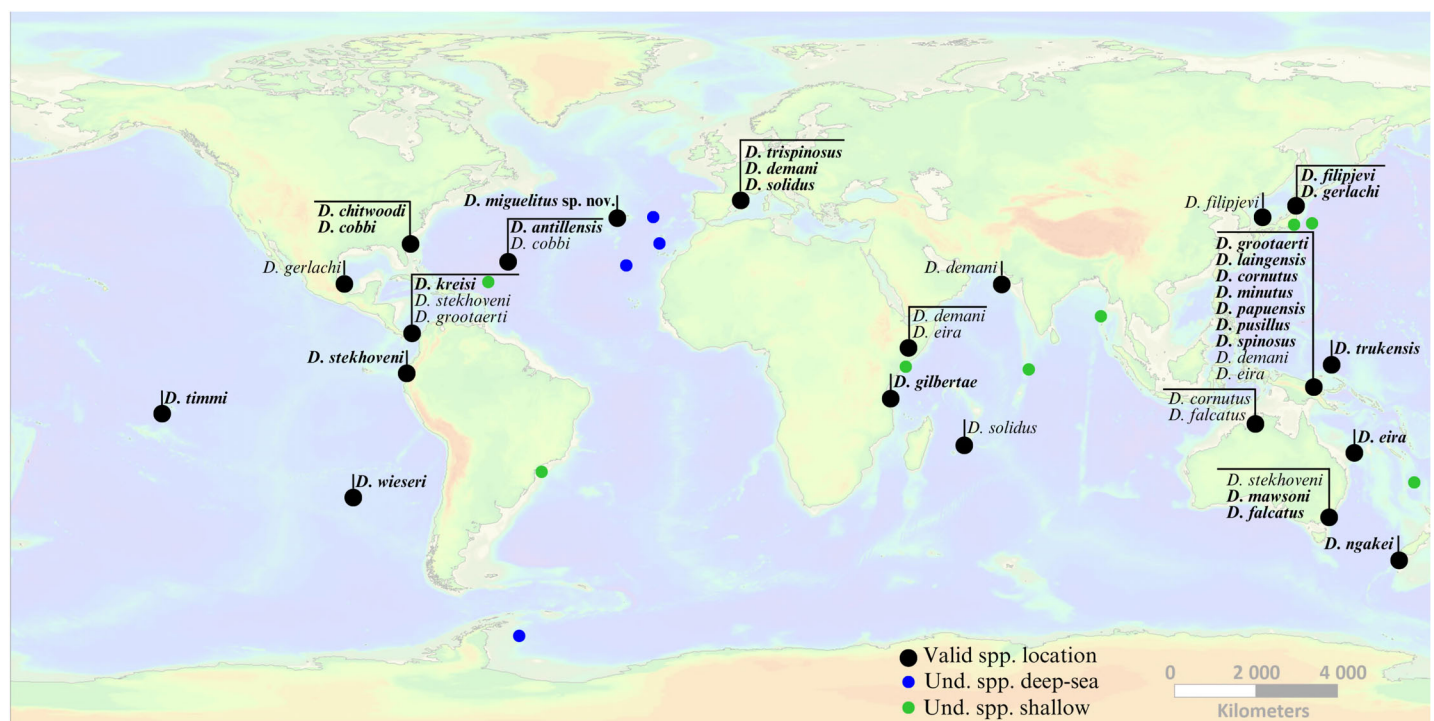
Figure 7 Global occurrence locations of the genus *Dracograllus*. Black dots indicate type localities of valid species (holotype names in bold, non-bold for paratypes). Colored circles represent occurrence locations of unidentified individuals or those classified as morphotypes (green points indicate these occurrences in shallow waters, 0–200 m, and blue points in deep-sea habitats, >200 m). Horizontal lines group morphotypes with overlapping occurrences or geographically close localities (*e.g.*, all species described for the Papua New Guinea region). For the precise locations, habitats, sampling details, and remarks on each valid and undetermined species globally, refer to Tables 4 and 5, respectively. *Nomen nudum* and invalid species in general not shown, but available in the genus review section.   Full-size 🖼 DOI: 10.7717/peerj.19585/fig-7

Dracograllus and even within the broader Draconematidae family. *Allen & Noffsinger (1978)* described *D. trispinosus* at 20 m depth, revealing the species occurrence in subtidal zones.

The Indian Ocean hosts fewer described species, yet their habitats share similarities with those in other regions. For instance, *D. demani* has been reported in tidal coral sands along the Malindi coast and also, in similar sandy habitats in the Pacific Ocean. Likewise, *D. eira* is known from both the Atlantic Ocean, where it inhabits subtidal sandy zones, and the Indian ocean, where it has been recorded in mangrove-associated sediments, demonstrating its ability to thrive in a range of coastal habitats. *D. solidus*, another widespread species, has been documented in the Atlantic, Pacific, and Indian oceans, consistently associated with coarse sand in subtidal regions.

Only a few studies have investigated the spatial distribution of *Dracograllus* in deep-sea ecosystems. Four morphotypes were found at the summit of the GSM in the Atlantic, which is a flat plateau covering more than 1,400 km^2, with 293 to 511 m depth (*Pfannkuche, Sommer & Kähler, 2000*). They exhibit significant abundance compared to other Draconematidae genus, with non-overlapping occurrences between each morphotype. The specific sedimentary processes on the GSM (*Levin & Nittrouer, 1987*), combined with the erosion of old coral reefs, create a coarse sedimentary environment,

with small and morphologically complex biogenic structures covering the substratum (*Pasenau, 1971*; *Nellen, 1998*). This wide variety of ecological niches would explain their high abundance and the co-occurrence of several species. Similarly, *Zeppilli et al. (2014)* reported several *Dracograllus* specimens at the Condor Seamount (CS), at 206 m depth, in the Azores archipelago (Northern Atlantic). The summit of this structure exhibited a highest species richness and dominance for several genus, clearly differing from the surrounding deep-sea habitats or along other CS habitats. The summit was the only area of the study where *Dracograllus* sp. 1 was present, a flat region, covered by biogenic structures such as sponge sediments or corals, as observed for most *Dracograllus* species. Similar results regarding Draconematidae species were obtained on other biogenic and sedimentary habitats (*Willems et al., 1982*; *Ndaro & O'lafsson, 1999*; *Raes & Vanreusel, 2006*; *Raes et al., 2007*; *Raes, Decraemer & Vanreusel, 2008*).

Draconematidae species were recently observed in samples collected from two deep hydrothermal vent fields, TAG and Snake Pit (SP) (*Spedicato et al., 2020*) located on the Mid-Atlantic Ridge. *Dracograllus* sp. was present in 50% of the SP samples, occurring in reddish sediments covered by polychaete tubes. In contrast, these features were absent or less evident at TAG, where only *Cephalochaetosoma* was recorded. Environmental conditions differed significantly between the vent fields. The total sulfur content in the sediment profiles (0–5 cm) was higher at SP than at TAG and the oxygen penetration about ten times lower at SP. High concentrations of sulfur can lead to death due to the inhibitory action of H_2S on cytochrome c oxidase, an essential enzyme for aerobic respiration. This mechanism blocks the electron transport chain, disrupting ATP production and resulting in metabolic collapse (*Bagarinao, 1992*). However, some nematode species have developed strategies to cope with sulfide toxicity, such as the oxidation of H_2S into elemental sulfur and its deposition in the epidermis, a process observed in *Oncholaimus campylocercoides* (*Thiermann, Vismann & Giere, 2000*). This ability to accumulate and later remove elemental sulfur may enable nematodes to colonize sulfide-rich environments, exploiting niches where most organisms cannot survive. Moreover, body elongation and a higher surface-to-volume ratio may help them cope with low O_2 levels in habitats with limited oxygen availability (*Vanreusel et al., 2010b*).

The non-overlapping distribution of *Dracograllus* species at deeper sites suggests that each species may have specific habitat requirements, influenced by both the nature and composition of the substratum, as well as the level of hydrothermal activity. The type-habitat of *D. miguelitus* **sp. nov.**, is characterized by low hydrothermal influence compared to active sites at the Lucky Strike (LS) vent field (*Chavagnac et al., 2018*). However, residual venting activity is still present, evidenced by the presence of manganese oxide-hydroxide and high CH4 concentrations measured above the substratum in one of the samples. Environmental conditions, including sediments rich in sulfide minerals, can stimulate microbial communities, which are essential as primary producers in these deposits (*Van Gaever et al., 2009*). This creates a higher food resource availability and provides structural conditions suitable for the occurrence of Draconematidae species, including *D. miguelitus* **sp. nov.**, classified as microbial feeders. In summary, the residual hydrothermal activity likely promotes microbial growth, a significant food source for

bacterivores and microbial feeders like *D. miguelitus* **sp. nov**. and most Draconematidae species. Moreover, the presence of biogenic structures like microbial mats, appear to play a role in the distribution of *Dracograllus* species. These species are capable of using adhesive tubes to anchor to these structures and may also feed on them (*Raes et al., 2007*).

Prior to the description of *D. miguelitus* **sp. nov.**, the Snake Pit species were the deepest-known representatives of the genus, found at depths between 3,480–3,570 m.

Biogeography and evolutionary perspectives

Several species of *Dracograllus*, and Draconematidae in general, have been found in only a few locations beyond their type habitats. However, nematologists agree that cosmopolitanism is common among various species and groups of marine nematodes (*Decraemer, Gourbault & Helléouet, 2001*). As reflected by *Gad (2009)*, based on Draconematidae species, one important starting point to determine the origins of these species is to identify their closest relatives and where they occur. In fact, some of the closely related species of *Dracograllus miguelitus* **sp. nov.** (*D. demani* and *D. minutus*) inhabit coastal and sublittoral environments of the Mediterranean Sea. These Mediterranean regions could be the source of this species, as surface currents transport waters from Gibraltar toward the Azores and upper regions of the North Atlantic (*Dietrich et al., 1975*; *Brenke, 2002*). Drifting-buoy experiments have confirmed that Mediterranean water eddies travel westward from Gibraltar across the Atlantic (*Richardson, 1996*). Such westward flows also occur at approximately 900 m depth, facilitating the transport of fauna, including meiofauna, which may drift as eggs, juveniles, or adults attached to marine snow (*Pingree, García-Soto & Sinha, 1999*; *Gad & Schminke, 2004*). This may also be the case for some *Prochaetosoma* species, as congeners have also been recorded in the Mediterranean. Other potential source regions, such as the coasts of Mauritania or Morocco, remain unconfirmed due to the absence of Draconematidae records from these areas. If such transport occurred, it would also depend on Mediterranean water flows (*Gad, 2009*).

Studies by *Gad (2009)* on the Great Meteor Seamount, *Zeppilli et al. (2014)* on the Condor Seamount, and *Spedicato et al. (2020)* on the TAG and Snake Pit vent fields identified closely related species in various deep-sea habitats along the northern MAR. Fifteen Draconematidae species, spanning several genera—including *Draconema, Paradraconema, Eudraconema, Prochaetosoma, Cephalochaetosoma*, and *Tenuidraconema*—were recorded on the GMS plateau, located 500 km from the Lucky Strike vent field. Remarkably, fourteen of these species were new to science, including four *Dracograllus* morphotypes (Table 5). In the CS (~300 km from LS), a rich and exclusive nematode community was documented, with 35 species distributed across genera such as *Akanthepsilonema, Apenodraconema, Bathychaetosoma, Dracograllus*, and others. Similarly, *Spedicato et al. (2020)* observed several Draconematidae specimens from three genera: *Cephalochaetosoma, Dinetia*, and *Dracograllus*.

Both hydrothermal vents and seamounts can be considered true oases of life compared to the surrounding deep-sea environment (*McClain et al., 2012*), emphasizing their importance for biogeographic studies, particularly for taxa that exhibit some degree of

Table 5 Global distribution, habitats, and environmental characteristics of unidentified *Dracograllus* sp.

Ocean	Site	Coords.	Habitat	Substratum type	Morphospecies	Reference
Atlantic ocean	Great Meteor Seamount	30°00′N, 28°30′W.	Plateau of the seamount, with 1,465 km2	Calcareous biogenic sands	*Dracograllus sp.4; Dracograllus sp.5; Dracograllus sp.6; Dracograllus sp.7*	*Gad (2009)*
	Condor Seamount	38°32.949′N, 29°02.879′W.	Summit of the seamount, at 206 m depth.	Large rocky outcrops, gravels, and coarse bioclastic deposits	*Dracograllus* sp.	*Zeppilli et al. (2014)*
	Snake Pit vent field	23°22.0′N, 44°57.0′W.	Sampling located 70 m from one black smoker. Depth between 3.480 m and 3.570 m	Reddish sediments covering the corer, with several polychaete tubes and individuals	*Dracograllus* sp.	*Spedicato et al. (2020)*
	Anse Laborde, Guadeloupe island	16°29.2′N, 61°30.3′W	Intertidal beach zone with high hydrodynamic activity.	Composed of detrital fragments, mostly carbonates	*Dracograllus* sp. 1	*Decraemer & Gourbault (1986), Renaud-Mornant & Gourbault (1981)*
	Raisins, clairs, Guadeloupe	16.24892°N, 61.28345°W	Sandy beach on the characterized by a low sandy ridge (2 to 3 m in height) facing frequent waves and subject to significant coastal erosion	Sediments consist of a low sandy ridge, with a "beach-rock" (sandstone) layer along the coastline.	*Dracograllus* sp. 2 and *Dracograllus* sp. 3	*Decraemer & Gourbault (1986), Renaud-Mornant & Gourbault (1981)*
	La Marie Galante.	15°55′59.99″N, 61°15′60.00″W	Sandy Beach with a topography that includes a low sand ridge parallel to the shoreline and sparse vegetation	Sandy beach composed of sediments ranging from fine volcanic sands to coarse organogenic sands.	*Dracograllus* sp. 4	*Decraemer & Gourbault (1986), Renaud-Mornant & Gourbault (1981)*
	Guadeloupe	15.912°N, 61.269°W	Sandy Beach, intertidal zone.	Substratum composed of sand, from medium to very coarse sediments. Highly impacted beach region subject to anthropogenic pressures.	*Dracograllus* sp.	*Maria et al. (2008)*
	Guanabara Bay, Rio de Janeiro, Brazil.	22°24′ S–22°57′S, 42°33′ W–43°19′W				
Pacific ocean	Munseon Island, Jjeudo, Korea	33°13′66″N, 126°34′18″E	Subtidal zone, 37 m deep.	Sampling based on washings of shallow subtidal detritus and coarse sediments	*Dracograllus* sp. 1	*Rho & Min (2011)*
	Geomundo Island, Jeonranamd, Korea	34°05′57″N, 127°14′84″E	Intertidal zone, associated with invertebrates	Substratum with associated invertebrates	*Dracograllus* sp. 2	*Rho & Min (2011)*
	Volcanic Island of Moorea, French Polynesia	(17°30′ S–149°50′W)	Flat beaches surrounded by a large coral reef	Sediments with coarse coral sand	*Dracograllus* sp. 1 e *Dracograllus* sp. 2	*Gourbault, Warwick & Helléouet (1995)*

Table 5 (continued)

Ocean	Site	Coords.	Habitat	Substratum type	Morphospecies	Reference
Indian ocean	Gazi Kenya	-4.4222°S, 39.5050°E	Sandy beach, intertidal zone	Sample taken in mangrove region, with *Ceriops sp.* tree	*Dracograllus* spec.	*Verschelde & Vincx (1993)*
	Chidiyatapu, South Andaman Island, India	11°29′30″N–11°30′34″N, 92°35′10″E–92°42′30″E	Rocky coastal area	Sediments associated with several seagrasses patches (*Thalassia hempirichi, Halodule uninervis* and *Halophila ovalis*)	*Dracograllus sp.*	*Naufal & Padmavati (2018)*
	Marina Park, Andaman Islands	11°40′15.39″N, 92°45′39.16″E	Sublitoral sediments	Substratum composed of silty-sand and clayey-sand	*Dracograllus sp.*	*Arunima et al. (2023)*
	Huvadhoo Atoll, Maldives	08°33′20.88″N, 73°81′4.76″E	Central atoll region	Sediments with coarse and gravelly sand, at 61 m deep.	*Dracograllus sp.*	*Semprucci et al. (2014)*
Southern ocean	Halley Bay, Weddel Sea	74°S–75°S, 25°W–29°W	Shelf break region, 500 m deep	Sediment poorly to extremely poorly sorted, with significant variations in grain size, with presence of pellite and gravel	*Dracograllus sp.*	*Vanhove, Arntz & Vincx, 1999*

habitat exclusivity, as observed in Draconematidae in the North Atlantic. Another intriguing aspect of Draconematidae in these regions is their morphological variability, which may reflect underlying biogeographic processes (*Costello & Chaudhary, 2017*). For example, in *Dracograllus* species from the GMS, individuals from the southern part of the plateau possess a fully divided cephalic capsule (helmet), whereas those from the northern part have a partially divided one (*Gad, 2009*). Additionally, there are variations in the number of SlATs and SvATs. Several other distinctive traits were reported, including the presence of eight strong spines around the vulva in *Draconema* sp. 1, a long and conical cephalic capsule in *Cephalochaetosoma* sp. 10, and extra-wide annules in the pharyngeal region of *Prochaetosoma* sp. 12. None of these distinctive traits were observed in Draconematidae species from LS (*Tchesunov, 2015*; W Johnson, 2025, unpublished data).

The intrageneric variation in the helmet among *Dracograllus*, along with the non-overlapping distributions of several Draconematidae genera and species across the CS, GMS, Snake Pit, and LS, and this may be related to an ongoing speciation process (*George, 2004*; *Gad, 2004*; *Gad, 2009*), similar to what was observed by *George & Schminke (2002)* and *Gad & Schminke (2004)* in copepods and macrofaunal species, respectively. In fact, when closely related species exhibit significant morphological variations within small geographic regions, it suggests that species may be arising through micro-allopatric speciation, where populations diverge due to localized environmental differences, leading to subtle, but sometimes crucialmorphological distinctions (*Rundle & Nosil, 2005*). As these populations adapt to specific ecological niches, genetic divergence and reproductive isolation may drive the emergence of new species, highlighting the importance of understanding local biodiversity and the environmental factors influencing species differentiation.

Given the known limitations of morphology-based taxonomy, such as cryptic diversity and convergent evolution, future studies integrating molecular markers, such as COI or 18S, will be crucial for validating the observed patterns and refining our understanding of species connectivity and dispersal (*Palmer, 1988a*, *1988b*; *De Ley et al., 2005*; *Bhadury et al., 2006*; *Derycke et al., 2010*; *Curini-Galletti et al., 2012*; *Ahmed et al., 2015*; *Martínez García et al., 2023*). Despite these challenges, our findings, together with the limited existing data on species distributions, suggest that both oceanic currents and local conditions and adaptations may play a role in shaping Draconematidae distributions. This highlights the need for further interdisciplinary approaches to fully elucidate the evolutionary and ecological processes governing meiofaunal diversity in deep-sea environments.

Inactive vent structure remarks and conservation implications

Hydrothermal vents have been the focus of numerous ecological studies since their discovery in 1977. These investigations have significantly enhanced our understanding of the structure and dynamics of benthic communities and the role of environmental conditions at various spatial and temporal scales (*Godet, Zelnio & Van Dover, 2011*). These habitats are known for their unique biogeochemical characteristics, which include commercially valuable mineral resources such as iron, copper, and zinc (*Van Dover, 2019*). However, the prospect of mining these sites poses serious environmental threats, including

permanent alterations in the local topography and removal of habitats (*Boschen et al., 2013*). Furthermore, mining could release toxic metals, disrupt ecological functions, and hinder the recruitment and recovery of sessile invertebrates, particularly in regions where hard substrata are limited (*Van Dover, 2019*).

While the fauna of active sites has been the focus of most vent studies, that of inactive sites is virtually unknown. Few studies report the presence of filter-feeders on the relief created by these mineral-rich mounds (*Boschen et al., 2013*; *Van Dover, 2019*). Moreover, it is suspected that these mineral deposits may host totally different communities than those found at active vents. This is supported by an eDNA study by *Cowart et al. (2020)* on the Lucky Strike vent field, which observed significantly higher diversity (OTUs—Operational Taxonomic Units) in both inactive and peripheral regions compared to active ones, as well as notably distinct communities among the active, inactive, and peripheral areas. While inactive vent systems differ from active ones, both of them face significant threats from deep-sea mining, with potentially severe consequences for biological communities and ecosystem functioning. This challenge is exacerbated by the limited knowledge on these habitats and their associated communities, particularly meiofaunal organisms, which are often overlooked in ecological studies. These knowledge gaps may hinder the development of effective management and conservation strategies (*Menini et al., 2023*).

By documenting the species present at inactive vents, researchers can better assess their ecological roles and connections with neighboring active systems. The discovery of *Dracograllus miguelitus* **sp. nov.** at an inactive vent structure exemplifies the biodiversity hidden in these understudied environments and highlights the urgent need for species-level research. Such findings are crucial for balancing conservation priorities with industrial ambitions, ensuring that management strategies are grounded in a comprehensive understanding of ecosystem dynamics and connectivity.

CONCLUSIONS

The discovery of a new nematode species not only provides valuable taxonomic and ecological data on a poorly studied genus but also underscores the ecological significance of inactive hydrothermal structures. These habitats increasingly warrant attention in the face of deep-sea mining threats. Future research should aim to further investigate the biodiversity and ecological roles of nematodes and other meiofauna in inactive vent ecosystems, integrating these findings into conservation and management strategies.

While these findings advance our understanding of vent nematode biodiversity, the study is limited to a single structure. Broader exploration across diverse hydrothermal regions and inactive structures and areas is essential to fully understand the genus distribution, biogeography, and ecological roles. Notably, the presence of *D. miguelitus* **sp. nov.** on an inactive structure may result from dispersal events from nearby areas. This highlights specific adaptations to both substratum type and heterogeneity, as well as hydrothermal influences, which require further in-depth study. In conclusion, this study emphasizes the importance of incorporating species-level data into hydrothermal vent research and highlights the urgent need for proactive conservation measures to safeguard

the biodiversity of all types of hydrothermal habitats in the face of increasing anthropogenic pressures.

Dichotomous key to *Dracograllus* valid species

The dichotomous key was constructed based on previous studies (*Allen & Noffsinger, 1978*; *Decraemer, Gourbault & Backeljau, 1997*; *Min et al., 2016*). The complete list for the description of valid *Dracograllus* species is listed in the reference section.

1. Four CATs on rostrum .... ***D. miguelitus* sp. nov**.

   - More than four CATs on rostrum 2

2. Without sublateral cephalic acanthiform setae on rostrum 3

   - With one pair of bilateral cephalic acanthiform setae on mid-rostrum .... ***D. stekholveni***

3. Males with 3–4 preanal corniform setae; 10–11 CATs. Females with 10 CATs: SlATn 18, SvATn 13–16 .... ***D. cornutus***

   - Males without preanal corniform setae; more CATs. Females with larger numbers of PATs... 4

4. Males with 7–8 short stiff setae in subventral rows just anterior to SvATl; spicules 39 μm long. Females with 24 SlAT, including 2 tubes posterior to the anus. Both sexes with a swollen pharyngeal region representing 22% of the total body length ... ***D. gerlarchi***

   - Males with 3–4 short stiff setae in subventral rows just anterior to SvATl; spicules 71 μm long. Females with 21 SlAT, including 3 tubes posterior to the anus. Swollen pharyngeal region 13–14% of total length .... ***D. falcatus***

5. Six CATs on rostrum; males with 5 SlAT, 2–3 SvAT; total length 290 μm; spicules 18 μm .... ***D. minutus***

   - Eight CATs on the rostrum. Number of PAT higher in males; spicule typically long 6

6. All CATs adjacent to or posterior to the amphideal fovea........................... 7

   - All CATs anterior to the amphideal fovea .... ***D. eira***

7. Males with preanal corniform setae; slender, conspicuously long and short SlAT alternating in both sexes .... ***D. trispinosum***

   - Males without preanal corniform setae; SlAT without alternating long and short tubes in both sexes 8

8. Several somatic setae in the posterior body region with spiny cuticular insertion and non-annulated tail tip representing 59% of tail length .... ***D. spinosus***

   - Somatic setae with spiny insertion collar 9

9. Some somatic setae pedicellate; pedicels 1–8 μm long.............................. 10

   - Somatic setae without pedicels... 13

10. Males with 5–9 SlAT; females with 6–12 SlAT, all anterior to the anus; 9–14 SvAT.. 11

- Males with 12–24 SlAT; females with 15 SlAT (1 posterior to anus) and 16 SvAT .... ***D. mawsoni***

11. Males with 5–7 SlAT; females with 9–13 SvAT 12

- Males with 9 SlAT; females with 14 SlAT .... ***D. cobbi***

12. Males and females with pedicellate setae in ventrosublateral row just anterior to SlAT; spicules 45–53 µm; females with 6–8 SlAT .... ***D. demani***

- Without pedicellate setae in ventrosublateral rows; spicules 36 µm; females with 12 SlAT .... ***D. kreisi***

13. Annulated body cuticle without ornamentation 14

- Annulated body cuticle ornamented with spines, dots, and vacuoles 15

14. Amphids long, inverted U-shaped in both sexes; males with 10 SlAT, 11 SvAT; spicules 29 µm; females with 11–13 SlAT and 9–11 SvAT .... ***D. papuensis***

- Amphids sexually dimorphic: loop-shaped in males, elongated unispiral in females; males with 7 SlAT, 11 SvAT; spicules 46 µm; females with 8–11 SlAT and same for SvAT .... ***D. solidus***

15. Body cuticle with vacuolar and granular ornamentation .... ***D. wieseri***

- Body cuticle ornamented with dots and spines 16

16. Body annules ornamented with two rows of dots 17

- Spiny ornamentation of the body cuticle 18

17. Amphids long, oblique loop-shaped in females; tail slender (tail/abd = 5.6) .... ***D. chitwoodi***

- Amphids inverted U-shaped in females; tail/abd = 3.9 .... ***D. timmi***

18. Amphids long, inverted U-shaped, as long as the rostrum 19

- Amphids short and wide, inverted U-shaped .... ***D. antillensis***

19. Short body (L = 310 µm); faint rostrum ornamentation; body annules with minute spines; spicule 26 µm; males with 6 SvAT .... ***D. pusillus***

- Body > 400 µm; spiny rostrum ornamentation; longer spicules; more than 6 SvAT in males 20

20. Long swollen pharyngeal region; amphids inverted U-shaped in males and elongated unispiral in females .... ***D. laingensis***

- Shorter, wider swollen pharyngeal region; amphids U-shaped in both sexes; spicules 68 µm .... ***D. grootaerti***

21. Body annules with dot-like punctations; no anal flap; females with two pairs of paravulvar setae (anterior and posterior to vulva, 5–6 µm) .... ***D. filipjevi***

- Anal flap present; females with different number/position of paravulvar setae 22

22. Large spaces between body annules; females without paravulvar setae .. ***D. gilbertae***

- Body annules closely spaced; females without paravulvar setae 23

23. Body annules without ornamentation; paravulvar setae absent .... ***D. ngakei***

- Paravulvar setae present; body annules with ornamentation 24

24. Body annules with numerous ridges and spiny protrusions, denser in lateral fields. Males with large loop-shaped amphids with ventral branch longer than dorsal, extending to the first body annule .... ***D. trukensis***

Abbreviations

The terminology used for the description and measurements was according to *Min et al. (2016)*, *Leduc & Zhao (2016)* and the classical approach by *de Man (1880)*. The abbreviations used are as follows:

L	body length
a	ratio body length/body maximum width
b	ratio body length/pharynx length
c	ratio body length/tail length
c'	ratio tail length/anal body diameter
C. m.	constrictor muscles of the vulvar region
abd	anal body diameter
Amphid from ant	distance from amphid to anterior end
Amphid. Length	amphideal length
Amphid. Width	amphideal width
Amphid./cbd (%)	amphideal length relative to the corresponding body diameter in %
CATs	cephalic adhesive tubes
CATl	length of cephalic adhesive tubes
CATn	number of cephalic adhesive tubes
Gub. Apoph. Length	gubernaculum apophysis length
Head diam.	head diameter
Max. body diam. Mb.	maximum body diameter at mid-body region
Max. body diam. Phar.	maximum body diameter at pharynx level
Min. body diam. Mb.	minimum body diameter at mid-body region
Non. ann. T. length	non-annulated tail tip length
Non. ann. T. length (%)	percentage of non-annulated tail tip relative to total tail length
Ov.	ovaries
PATs	posterior adhesive tubes
Phar. bulb diam. (ant.)	anterior pharyngeal bulb diameter
Phar. bulb diam. (post.)	posterior pharyngeal bulb diameter
Phar. length	pharynx length
PS	paravulvar setae
PS length	paravulvar setae length
SlAT	sublateral adhesive tubes
SvAT	subventral adhesive tubes
SlATn	number of sublateral adhesive tubes
SvATn	number of subventral adhesive tubes

Competing Interests

The authors declare that they have no competing interests.

Author Contributions

- William Johnson da Silva performed the experiments, analyzed the data, prepared figures and/or tables, authored or reviewed drafts of the article, and approved the final draft.
- Daniela Zeppilli analyzed the data, authored or reviewed drafts of the article, and approved the final draft.
- Valentin Foulon performed the experiments, analyzed the data, prepared figures and/or tables, authored or reviewed drafts of the article, and approved the final draft.
- Pierre-Antoine Dessandier analyzed the data, authored or reviewed drafts of the article, and approved the final draft.
- Marjolaine Matabos conceived and designed the experiments, authored or reviewed drafts of the article, and approved the final draft.
- Jozee Sarrazin conceived and designed the experiments, authored or reviewed drafts of the article, and approved the final draft.

Data Availability

The following information was supplied regarding data availability:

All specimens are registered under MNHN-BN511 at the Muséum National d'Histoire Naturelle (MNHN).

Supplemental Information

Supplemental information for this article can be found online at http://dx.doi.org/10.7717/peerj.19585#supplemental-information.

REFERENCES

Ahmed M, Sapp M, Prior T, Karssen G, Back M. 2015. Nematode taxonomy: from morphology to metabarcoding. *Soil Discussions* **2(2)**:1175–1220 DOI 10.5194/soild-2-1175-2015.

Allen MW, Noffsinger EM. 1978. A revision of the marine nematodes of the superfamily Draconematoidea Filipjev, 1918 (Nematoda: Draconematina). *University of California Publications in Zoology* **109**:1–133.

Arunima TA, Afnan NM, Swathi V, Heera NH, Shah KS, Mohan PM. 2023. Distribution of meiofauna in the sublittoral sediments of the tropical island ecosystem, off Port Blair, Andaman Sea. *Indian Journal of Geo-Marine Sciences (IJMS)* **52(3)**:130–144.

Bagarinao T. 1992. Sulfide as an environmental factor and toxicant: tolerance and adaptations in aquatic organisms. *Aquatic Toxicology* **24(1–2)**:21–62 DOI 10.1016/0166-445x(92)90015-f.

Bhadury P, Austen MC, Bilton DT, Lambshead PJD, Rogers AD, Smerdon GR. 2006. Development and evaluation of a DNA-barcoding approach for the rapid identification of nematodes. *Marine Ecology Progress Series* **320**:1–9 DOI 10.3354/meps320001.

Boschen RE, Rowden AA, Clark MR, Gardner JPA. 2013. Mining of deep-sea seafloor massive sulfides: a review of the deposits, their benthic communities, impacts from mining, regulatory frameworks, and management strategies. *Ocean & Coastal Management* **84(Suppl.)**:54–67 DOI 10.1016/j.ocecoaman.2013.07.005.

Brenke N. 2002. The benthic community of the Great Meteor Bank. In Oceanography and ecology of seamounts—indications of unique ecosystems. In: *Documents and ICES Annual Report for 2002, ICES ASC CM 2002/M-30*. Copenhagen, Denmark: International Council for the Exploration of the Sea (ICES), 1–12.

Cannat M. 2018. MOMARSAT, 2018 cruise. RV L'Atalante DOI 10.17600/18000514.

Chavagnac V, Fontaine F, Cannat M, Ceuleneer G. 2018. Deep-sea observatory EMSO-Azores (Lucky Strike, 37o17'N MAR): impact of fluid circulation pathway on chemical hydrothermal fluxes. *Geochemistry, Geophysics, Geosystems* **19(11)**:4455–4478 DOI 10.1029/2018GC007765.

Clasing E. 1980. Postembryonic development in species of Desmodoridae, Epsilonematidae, and Draconematidae. *Zoologischer Anzeiger* **204**:37–344.

Cobb NA. 1913. *Draconema*: a remarkable genus of marine free-living nematodes. *Journal of the Washington Academy of Sciences* **3(5)**:145–149 DOI 10.5962/bhl.part.20322.

Cobb NA. 1929. The ambulatory tube and other features of the nema *Draconema cephalatum*. *Journal of the Washington Academy of Sciences* **19**:255–260 Reprinted in Contributions to a Science of Nematology, 22, 413–418.

Cobb NA. 1933. New nemic genera and species, with taxonomic notes (M. V. Cobb, Ed.). *Journal of Parasitology* **20(2)**:81–94.

Costello MJ, Chaudhary C. 2017. Marine biodiversity, biogeography, deep-sea gradients, and conservation. *Current Biology* **27(11)**:R511–R527 DOI 10.1016/j.cub.2017.04.060.

Cowart DA, Matabos M, Brandt MI, Marticorena J, Sarrazin J. 2020. Exploring environmental DNA (eDNA) to assess biodiversity of hard substratum faunal communities on the Lucky Strike vent field (Mid-Atlantic Ridge) and investigate recolonization dynamics after an induced disturbance. *Frontiers in Marine Science* **6**:1–21 DOI 10.3389/fmars.2019.00783.

Curini-Galletti M, Artois T, Delogu V, De Smet WH, Fontaneto D, Jondelius U, Leasi F, Martínez A, Meyer-Wachsmuth I, Nilsson KS, Tongiorgi P, Worsaae K, Todaro MA. 2012. Patterns of diversity in soft-bodied meiofauna: dispersal ability and body size matter. *PLOS ONE* **7(3)**:e33801 DOI 10.1371/journal.pone.0033801.

De Busserolles F, Sarrazin J, Gauthier O, Gélinas Y, Fabri MC, Sarradin PM, Desbruyéres D. 2009. Are spatial variations in the diets of hydrothermal fauna linked to local environmental conditions? *Deep Sea Research Part II: Topical Studies in Oceanography* **56**:1649–1664.

De Coninck LA. 1965. Classe des Nématodes-Systématique des Nématodes et sous-classe des Adenophorea. *Traité de Zoologie* **4(2)**:586–681.

Decraemer W. 1988. *Dracograllus* (Nematoda: Draconematidae) from Papua New Guinea, with descriptions of new species. Leopold III Biological Station, Laing Island—Contribution no. 158. *Bulletin of the Institute Royal Sciences Naturelles de Belgique (Biologie)* **58(3)**:5–27 DOI 10.1071/it9870231.

Decraemer W, Gourbault N. 1986. Marine nematodes from Guadeloupe and other Caribbean Islands. II. Draconematidae. *Zoologica Scripta* **15(2)**:107–118 DOI 10.1111/j.1463-6409.1986.tb00214.x.

Decraemer W, Gourbault N, Backeljau T. 1997. Marine nematodes of the family Draconematidae (Nemata): a synthesis with phylogenetic relationships. *Hydrobiologia* **364(1)**:45–68 DOI 10.1023/A:1003155424665.

Decraemer W, Gourbault N, Helléouet MN. 2001. Cosmopolitanism among nematodes: examples from Epsilonematidae. *Vie et Milieu/Life & Environment* **51(1)**:11–19.

De Grisse AT. 1969. Redescription ou modifications de quelques techniques utilisées dans l'étude des nématodes phytoparasitaires. *Mededelingen van de Rijksfaculteit Landbouwwetenschappen Gent* **34**:351–369.

de Jesús-Navarrete A. *Catálogo de los nematodos acuáticos de vida libre, de la cuenca de la laguna de términos campeche.*

De Ley P, Tandingan De Ley I, Morris K, Abebe E, Mundo-Ocampo M, Yoder M, Heras J, Waumann D, Rocha-Olivares A, Burr AJ, Baldwin JG, Thomas WK. 2005. An integrated approach to fast and informative morphological vouchering of nematodes for applications in molecular barcoding. *Philosophical Transactions of the Royal Society B: Biological Sciences 360* **1462(1462)**:1945–1958 DOI 10.1098/rstb.2005.1726.

de Man JG. 1880. Über einige neue oder noch unvollständig bekannte Arten von frei in der reinen Erde lebenden Nematoden (1. Supplement zu den Aufsatz auf S. 1 dieses Bandes). *Tijdschr. ned. dierk. Vereen.* **5**:138–143.

Derycke S, Vanaverbeke J, Rigaux A, Backeljau T, Moens T. 2010. Exploring the use of cytochrome oxidase c subunit 1 (COI) for DNA barcoding of free-living marine nematodes. *PLOS ONE* **5(10)**:e13716 DOI 10.1371/journal.pone.0013716.

Dietrich CD, Kalle K, Kraus W, Siedler G. 1975. *Allgemeine Meereskunde.* Berlin & Stuttgart: Gebrüder Bornträger.

Dinet A, Grassle F, Tunnicliffe V. 1988. Premières observations sur la méiofaune des hydrothermaux de la dorsale Est-Pacifique (Guaymas, 21°N) et de l'Explorer Ridge. *Oceanologica Acta* **8(5)**:7–14.

Filipjev IN. 1918. Free-living marine nematodes of the Sevastopol area. *Transactions of the Zoological Laboratory and the Sevastopol Biological Station of the Russian Academy of Sciences* **Series II(4)**:1–2.

Filipjev IN. 1922. Encore sur les Nématodes libres de la mer Noire. *Travaux de l'Institut Zoologique de l'Académie des Sciences de Stravropole* **1**:83–184.

Filipjev IN. 1934. Miscellanea Nematologica. I. Eine neue Art der Gattung Neoaplectana Steiner nebst Bemerkungen über die systematische Stellung der letzteren. *Parasitologicheskii Sbornik Zoologicheskogo Instituta Akademii Nauk SSSR* **4**:229–240.

Flint HC, Copley JTP, Ferrero TJ, Van Dover CL. 2006. Patterns of nematode diversity at hydrothermal vents on the East Pacific Rise. *Cahiers de Biologie Marine* **47(4)**:365–370.

Foulon V, Malloci M, Zeppilli D. 2025. Nematode imaged with motorized binocular, laser scanning confocal microscope and lightsheet microscope. SEANOE DOI 10.17882/104251.

Gad G. 2004. Diversity and assumed origin of the Epsilonematidae (Nematoda) of the plateau of the Great Meteor Seamount. *Archive of Fishery and Marine Research* **51(1–3)**:30–42.

Gad G. 2009. Colonisation and speciation on seamounts: evidence from Draconematidae (Nematoda) of the Great Meteor Seamount. *Marine Biodiversity* **39(1)**:57–69 DOI 10.1007/s12526-009-0007-6.

Gad G, Schminke HK. 2004. How important are seamounts for the dispersal of meiofauna. *Archiv für Fischereiwissenschaft* **51(1–3)**:43–54.

George KH. 2004. Description of two new species of Bodinia, a new genus incertae sedis in Argestidae Por, 1986 (Copepoda, Harpacticoida), with reflections on argestid colonization of the Great Meteor Seamount plateau. *Organisms Diversity & Evolution* **4(4)**:241–254 DOI 10.1016/j.ode.2004.02.003.

George KH, Schminke HK. 2002. Harpacticoida (Crustacea, Copepoda) of the Great Meteor Seamount, with first conclusions as to the origin of the plateau fauna. *Marine Biology (Berl)* **141(5)**:887–895 DOI 10.1007/s00227-002-0878-6.

Gerlach SA. 1952. Nematoden aus dem Küstengrundwasser. *Abhandlungen der Mathematisch-Naturwissenschaftlichen Klasse der Akademie der Wissenschaften und der Literatur in Mainz* **6**:315–372.

Godet L, Zelnio KA, Van Dover CL. 2011. Scientists as stakeholders in conservation of hydrothermal vents. *Conservation Biology* **25(2)**:214–222 DOI 10.1111/j.1523-1739.2010.01642.x.

Gollner S, Miljutina M, Bright M. 2013. Nematode succession at deep-sea hydrothermal vents after a recent volcanic eruption with the description of two dominant species. *Organisms Diversity & Evolution* **13(3)**:349–371 DOI 10.1007/s13127-012-0122-2.

Gourbault N, Decraemer W. 1992. Marine nematodes from Polynesia: Epsilonematidae and Draconematidae. *Australian Journal of Marine and Freshwater Research* **43(4)**:663–681 DOI 10.1071/mf9920663.

Gourbault N, Warwick RM, Helléouet MN. 1995. A survey of intertidal meiobenthos (especially Nematoda) in coral sandy beaches of Moorea (French Polynesia). *Bulletin of Marine Science* **57(2)**:476–488.

Hoagland P, Beaulieu S, Tivey MA, Eggert RG, German C, Glowka L, Lin J. 2010. Deep-sea mining of seafloor massive sulfides. *Marine Policy* **34(3)**:728–732 DOI 10.1016/j.marpol.2009.12.001.

Humphris SE, Fornari DJ, Scheirer DS, German CR, Parson LM. 2002. Geotectonic setting of hydrothermal activity on the summit of Lucky Strike Seamount (37°17′N, Mid-Atlantic Ridge). *Geochemistry, Geophysics, Geosystems* **3(8)**:2001GC000284 DOI 10.1029/2001GC000284.

Husson B, Sarradin P-M, Zeppilli D, Sarrazin J. 2017. Picturing thermal niches and biomass of hydrothermal vent species. Ifremer, Archimer. Authors' manuscript available at https://archimer.ifremer.fr/doc/00341/45254/, also published by Deep-sea Research Part II-topical Studies In Oceanography. 137. 6–25 DOI 10.1016/j.dsr2.2016.05.028.

Inglis WG. 1968. Interstitial nematodes from St. Vincent's Bay, New Caledonia. In: *Expédition Française sur les Récifs Coralliens de la Nouvelle Calédonie.* Vol. 2. Saint-Jacques: Editions de la Fondation Singer-Polignac, Occasional Publications, 29–74.

Irwin-Smith VA. 1918. On the Chaetosomatidae, with descriptions of new species, and a new genus from the coast of New South Wales. *Proceedings of the Linnean Society of New South Wales* **42(1)**:757–814 DOI 10.1111/j.1096-3642.1798.tb00533.x.

Johnston TH. 1938. A census of free-living and plant-parasitic nematodes recorded as occurring in Australia. *Transactions of the Royal Society of South Australia* **62**:149–167.

Kito K. 1983. Deep-sea nematodes off Mindanao Island, the Philippines. I. Draconematidae. *Annotationes Zoologicae Japonenses* **56(1)**:27–41.

Koschinsky A, Garbe-Schönberg D, Sander S, Schmidt K, Gennerich HH, Strauss H. 2008. Hydrothermal venting at pressure-temperature conditions above the critical point of seawater, 5 S on the Mid-Atlantic Ridge. *Geology* **36(8)**:615–618 DOI 10.1130/G24726A.1.

Kreis HA. 1938. LXVII. Neue Nematoden aus der Südsee. *Videnskabelige Meddelelser fra Dansk naturhistorisk Forening* **101**:153–181.

Leduc D, Zhao Z. 2016. Phylogenetic relationships within the superfamily Desmodoroidea (Nematoda: Desmodorida), with descriptions of two new and one known species. *Zoological Journal of the Linnean Society* **176(3)**:511–536 DOI 10.1111/zoj.12324.

Levin LA, Baco AR, Bowden DA, Colaco A, Cordes EE, Cunha MR, Demopoulos AWJ, Gobin J, Grupe BM, Le J, Metaxas A, Netburn AN, Rouse GW, Thurber AR, Tunnicliffe V, Van Dover CL, Vanreusel A, Watling L. 2016. Hydrothermal vents and methane seeps: rethinking the sphere of influence. *Frontiers in Marine Science* **3(e76869)**:72 DOI 10.3389/fmars.2016.00072.

Levin LA, Nittrouer CA. 1987. Textural characteristics of sediments on deep seamounts in the eastern Pacific Ocean between 10° and 30°N. In: Keating B, Fryer P, Batiza R, Boehlert G, eds. *Seamounts, Islands, and Atolls (AGU Monograph Series).* Vol. 43. Washington, D.C.: American Geophysical Union, 187–203.

Maria TF, Esteves AM, Smol N, Vanreusel A, Decraemer W. 2008. Nematodes from sandy beaches of Guanabara bay, Rio de Janeiro, Brazil. *Biociências* **16(2)**.

Martínez García A, Bonaglia S, Di Domenico M, Fonseca G, Ingels J, Jörger K, Fontaneto D. 2023. Fundamental questions in meiofauna—how small but ubiquitous animals can help to better understand nature. EcoEvoRxiv DOI 10.32942/X2WP43.

McClain CR, Allen AP, Tittensor DP, Rex MA. 2012. Energetics of life on the deep seafloor. *Proceedings of the National Academy of Sciences* **109(38)**:15366–15371.

Menini E, Calado H, Danovaro R, Manea E, Halpin PN. 2023. Towards a global strategy for the conservation of deep-sea active hydrothermal vents. *npj Ocean Sustainability* **2(1)**:22 DOI 10.1038/s44183-023-00029-3.

Min W, Kim D, Decraemer W, Rho HS. 2016. *Dracograllus trukensis* sp. nov. (Draconematidae: Nematoda) from a seagrass bed (Zostera spp.) in Chuuk Islands, Micronesia, Central Western Pacific Ocean. *Ocean Science Journal* **51(3)**:343–354 DOI 10.1007/s12601-016-0030-z.

Naufal PJ, Padmavati G. 2018. Meiofaunal distribution and abundance from the intertidal seagrass patches of Chidiyatapu, Port Blair. *Indian Journal of Geo Marine Science* **47(2)**:2018.

Ndaro S, O'lafsson E. 1999. Soft-bottom fauna with emphasis on nematode assemblage structure in a tropical lagoon in Zanzibar, eastern Africa: I. Spatial variability. *Hydrobiologia* **405(0)**:133–148 DOI 10.1023/a:1003874122971.

Nellen W. 1998. Meteor 42/3 cruise report. Institut für Hydrobiologie und Fischereiwissenschaft der Universität Hamburg. *Available at* https://www.bodc.ac.uk/resources/inventories/cruise_inventory/reports/meteor42_98part3.pdf.

Nemys. 2024. Nemys: world database of Nematodes. *Available at* https://nemys.ugent.be (accessed 5 November 2024).

Ondreas H, Cannat M, Fouquet Y, Normand A, Sarradin P-M, Sarrazin J. 2009. Recent volcanic events and the distribution of hydrothermal venting at the Lucky Strike hydrothermal field, Mid-Atlantic Ridge. *Geochemistry, Geophysics, Geosystems* **10(2)**:1–18 DOI 10.1029/2008GC002171.

Palmer MA. 1988a. Dispersal of marine meiofauna: a review and conceptual model explaining passive transport and active emergence with implications for recruitment. *Marine Ecology Progress Series* **48**:81–91 DOI 10.3354/meps048081.

Palmer MA. 1988b. Ecological and evolutionary processes in the evolution of marine invertebrates. In: *Ecology and Evolution of Marine Invertebrates*. Dordrecht: Springer, 1–20.

Pasenau H. 1971. Morphometrische Untersuchungen an Hangterassen der Großen Meteorbank. *Meteor-Forschungsergebnisse C* **6**:69–82.

Pfannkuche O, Sommer S, Kähler A. 2000. Coupling between phytodetritus deposition and the small-sized benthic biota in the deep Arabian Sea: analyses of biogenic sediment compounds. *Deep Sea Research Part II: Topical Studies in Oceanography* **47(14)**:2805–2833 DOI 10.1016/S0967-0645(00)00050-3.

Pfannkuche O, Thiel H. 1988. Sample processing. In: Higgins RP, Thiel H, eds. *Introduction to the Study of Meiofauna*. Washington, D.C: Smithsonian Institution Press, 488.

Pingree RD, García-Soto RS, Sinha B. 1999. Position and structure of the subtropical/Azores front region from combined Lagrangian and remote sensing (IR/altimeter/SeaWIFS) measurements. *Journal of the Marine Biological Association of the United Kingdom* **79(5)**:769–792 DOI 10.1017/S002531549900096X.

Raes M, De Troch M, Ndaro SGM, Muthumbi A, Guilini K, Vanreusel A. 2007. The structuring role of microhabitat type in coral degradation zones: a case study with marine nematodes from Kenya and Zanzibar. *Coral Reefs* **26(1)**:113–126 DOI 10.1007/s00338-006-0184-8.

Raes M, Decraemer W, Vanreusel A. 2008. Walking with worms: Coral-associated epifaunal nematodes. *Journal of Biogeography* **35(12)**:2207–2222 DOI 10.1111/j.1365-2699.2008.01945.x.

Raes M, Vanreusel A. 2006. Microhabitat type determines the composition of nematode communities associated with sediment-clogged cold-water coral framework in the Porcupine Seabight (NE Atlantic). *Deep Sea Research Part I: Oceanographic Research Papers* **53(12)**:1880–1894 DOI 10.1016/j.dsr.2006.07.007.

Renaud-Mornant J, Gourbault N. 1981. Premiéres prospections meiofaunistiques en Guadeloupe. I. Les biotopes et leurs peuplements. *Bulletin du Muséum national d'histoire naturelle. Paris. 4é sér. 3* sec. **A(4)**:1011–1034.

Rho HS, Kim DS, Kim W. 2006. Redescription of free-living marine nematode, *Dracograllus filipjevi* Allen and Noffsinger, 1978 (Nematoda: Draconematidae) from Korea. *Ocean Science Journal* **41(3)**:163–173 DOI 10.1007/BF03022421.

Rho HS, Kim DS, Min WG. 2007. *Tenuidraconema tongaense* n. sp. (Nematoda: Draconematidae), a new free-living marine nematode from a seamount in the southwest Pacific Ocean. *Nematology* **9(4)**:545–560 DOI 10.1163/156854107781487233.

Rho HS, Min WG. 2011. Nematoda: Chromadorea: Desmodorida: Draconematidae, marine dragon nematodes. In: *Invertebrate Fauna of Korea.* Vol. 13. Incheon: National Institute of Biological Resources, 1–78.

Richardson PR. 1996. Tracking ocean eddies. In: Pirie RG, ed. *Oceanography*. Oxford: Oxford University Press, 200–212.

Rundle HD, Nosil P. 2005. Ecological speciation. *Ecology Letters* **8(3)**:336–352 DOI 10.1111/j.1461-0248.2004.00715.x.

Semprucci F, Burattini S. 2015. Re-description of *Craspodema reflectans* (Nematoda, Cyatholaimidae) using confocal laser scanning microscopy. *Zootaxa* **3972(3)**:407–418 DOI 10.11646/zootaxa.3972.3.6.

Semprucci F, Burattini S, Falcieri E, Balsamo M. 2017. A re-description of *Longicyatholaimus maldivarum* Gerlach, 1964 (Nematoda, Cyatholaimidae) with an emended identification key of the genus. *Zootaxa* **4323(1)**:96–108 DOI 10.11646/zootaxa.4323.1.7.

Semprucci F, Burattini S, Kim H, Hong JH, Lee W, Guidi L, Balsamo M. 2016. Application of confocal laser scanning microscopy in the taxonomy of free-living marine nematodes. *Microscopie* **26(2)**:48–57.

Semprucci F, Colantoni P, Sbrocca C, Baldelli G, Balsamo M. 2014. Spatial patterns of distribution of meiofaunal and nematode assemblages in the Huvadhoo lagoon (Maldives, Indian Ocean). *Journal of the Marine Biological Association of the United Kingdom* **94(7)**:1377–1385.

Shahina F, Nasira K, Firoza K, Erum YI. 2019. Overview of the nematode fauna of Pakistan. *Pakistan Journal of Nematology* **37(2)**:171–243.

Somerfield PJ, Warwick RM. 1996. Meiofauna in marine pollution monitoring programmes: a laboratory manual. Blackburn: Ministry of Agriculture, Fisheries and Food, Directorate of Fisheries Research.

Spedicato A, Sánchez N, Pastor L, Menot L, Zeppilli D. 2020. Meiofauna community in soft sediments at TAG and Snake Pit hydrothermal vent fields. *Frontiers in Marine Science* **7**:200 DOI 10.3389/fmars.2020.00200.

Stauffer H. 1924. Die Lokomotion der Nematoden. Beiträge zur Kausalmorphologie der Fadenwürmer. *Zoologischer Jahrbücher* **49**:1–118.

Stock SP, Nadler SA. 1998. Revised list of type specimens on deposit in the University of California Davis Nematode collection. *Journal of Nematology* **30(3)**:368.

Tchesunov AV. 2014. Order Desmodorida De Coninck, 1965. In: Schmidt-Rhaesa A, ed. *Handbook of Zoology: Gastrotricha, Cycloneuralia, Gnathifera. Volume 2: Nematoda.* Berlin, Boston: De Gruyter, 399–434.

Tchesunov AV. 2015. Free-living nematode species (Nematoda) dwelling in hydrothermal sites of the North Mid-Atlantic Ridge. *Helgoland Marine Research* **69(4)**:343–384 DOI 10.1007/s10152-015-0443-6.

Thiermann F, Vismann B, Giere O. 2000. Sulphide tolerance of the marine nematode Oncholaimus campylocercoides—a result of internal sulphur formation? *Marine Ecology Progress Series* **193**:251–259 DOI 10.3354/meps193251.

Tunnicliffe V. 1991. The biology of hydrothermal vents: ecology and evolution. *Oceanography and Marine Biology: An Annual Review* **29**:319–407.

Van Dover CL. 2019. Inactive sulfide ecosystems in the deep sea: a review. *Frontiers in Marine Science* **6**:461 DOI 10.3389/fmars.2019.00461.

Van Gaever S, Olu K, Derycke S, Vanreusel A. 2009. Metazoan meiofaunal communities at cold seeps along the Norwegian margin: Influence of habitat heterogeneity and evidence for connection with shallow-water habitats. *Deep Sea Research Part I: Oceanographic Research Papers* **56(5)**:772–785 DOI 10.1016/j.dsr.2008.12.015.

Vanhove S, Arntz W, Vincx M. 1999. Comparative study of the nematode communities on the southeastern Weddell Sea shelf and slope (Antarctica). *Marine Ecology Progress Series* **181**:237–256 DOI 10.3354/meps181237.

Vanreusel A, De Groote A, Gollner S, Bright M. 2010b. Ecology and biogeography of free-living nematodes associated with chemosynthetic environments in the deep sea: a review. *PLOS ONE* **5(8)**:e12449 DOI 10.1371/journal.pone.0012449.

Vanreusel A, Fonseca G, Danovaro R, Da Silva MC, Esteves AM, Ferrero T, Gad G, Galtsova V, Gambi C, Da Fonsêca Genevois V, Ingole B, Lampadariou N, Merckx B, Miljutin D, Miljutina M, Muthumbi A, Netto S, Portnova D, Radziejewska T, Raes M, Tchesunov A, Vanaverbeke J, Van Gaever S, Venekey V, Bezerra TN, Flint H, Copley J, Pape E, Zeppilli D, Arbizu M, Galeron J. 2010a. The contribution of deep-sea macrohabitat heterogeneity to global nematode diversity. *Marine Ecology* **31(1)**:6–20 DOI 10.1111/j.1439-0485.2009.00352.x.

Vanreusel A, Van den Bossche I, Thiermann F. 1997. Free-living marine nematodes from hydrothermal sediments: similarities with communities from diverse reduced habitats. *Marine Ecology Progress Series* **157(8)**:207–219 DOI 10.1371/journal.pone.0012449.

Verschelde D, Vincx M. 1993. Draconematidae (Nematoda, Desmodoroidea) from the coast of Kenya, East Africa. *Bulletin de l'Institut Royal des Sciences Naturelles de Belgique* **63**:25–53.

Willems KA, Vincx M, Claeys D, Vanosmael C, Heip C. 1982. Meiobenthos of a sublittoral sandbank in the Southern Bight of the North Sea. *Journal of the Marine Biological Association of the United Kingdom* **62(3)**:535–548 DOI 10.1017/S0025315400019731.

Zeppilli D, Bongiorni L, Serrão Santos R, Vanreusel A. 2014. Changes in nematode communities in different physiographic sites of the Condor Seamount (North-East Atlantic Ocean) and adjacent sediments. *PLOS ONE* **9(12)**:e115601 DOI 10.1371/journal.pone.0115601.

Zeppilli D, Vanreusel A, Pradillon F, Fuchs S, Mandon P, James T, Sarrazin J. 2015. Rapid colonisation by nematodes on organic and inorganic substrata deployed at the deep-sea Lucky Strike hydrothermal vent field (Mid-Atlantic Ridge). *Marine Biodiversity* **45(3)**:489–504 DOI 10.1007/s12526-015-0348-2.

Zullini A, Villa F. 2009. Redescription of three tobrilids (Nematoda) from Altherr's collection using confocal microscopy. *Journal of Nematode Morphology and Systematics* **8(2)**:121–132.